Nonlinear Aeroelastic Analysis of a High Aspect Ratio Wing in NASTRAN

Master of Science Thesis Report

Himanshu Anand

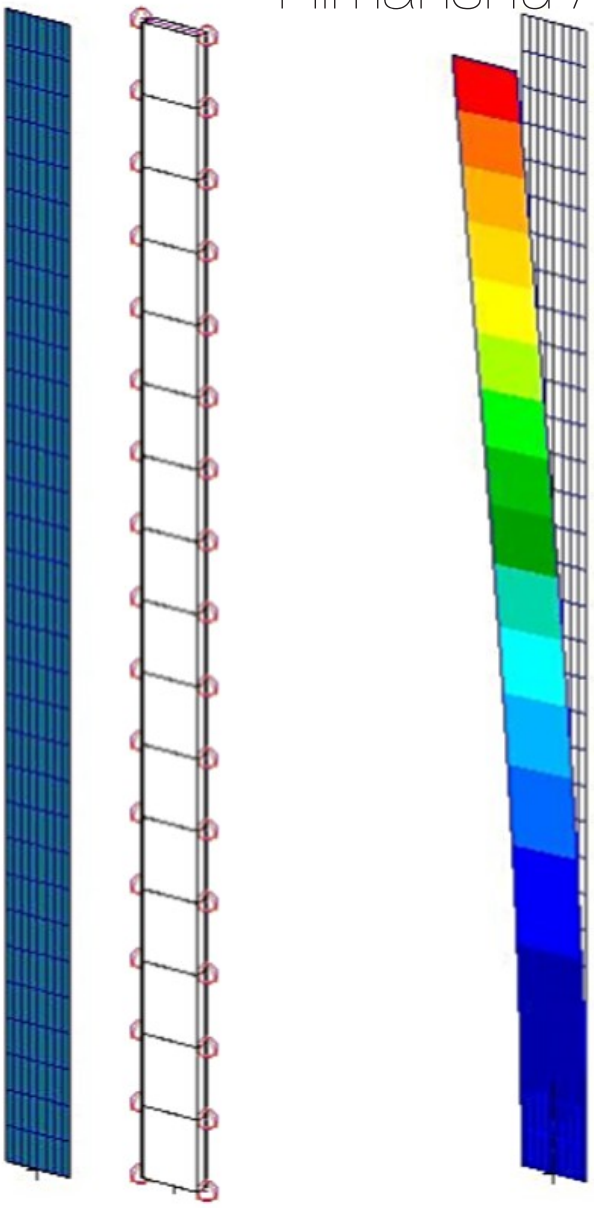

TU Delft

Nonlinear Aeroelastic Analysis of a High Aspect Ratio Wing in NASTRAN

Master of Science Thesis Report

by

Himanshu Anand

to obtain the degree of Master of Science

at the Delft University of Technology,

to be defended publicly on Tuesday April 29, 2019 at 9:00 AM.

Student number:	4468244	
Project duration:	August 1, 2017 – March 29, 2019	
Thesis committee:	Dr. ir. Roeland de Breuker,	TU Delft, supervisor
	Dr. ir. Roelof Vos,	TU Delft
	Dr. ing. Saullo Giovani Pereira Castro,	TU Delft
	Dr. Jurij Sodja,	TU Delft
	Ir. Paul Lancelot,	TU Delft

An electronic version of this thesis is available at http://repository.tudelft.nl/.

TU Delft

Acknowledgements

Most important endeavours in life are joint ventures where an individual succeeds only because of the efforts of the group of people that are supporting him or her. This thesis report would be incomplete without acknowledging the contributions of the many, many people who made it come to fruition.

First and foremost I would like to express my heartfelt thanks to my supervisor Dr Roeland de Breuker for his guidance trust, and patience over the last two years. Paul Lancelot, my day to day supervisor has put in nearly as much work in this thesis as I have. I thank him for his valuable advice and all his invaluable help.

I would also like to thank Dr Roelof Vos, Dr Saullo Castro and Dr Jurij Sodja for agreeing to be a part of my graduation committee at short notice, despite pressing engagements.

I am also grateful to Dr Breuker's PhD students Mario Natella and Darwin Rajpal for helping me with the validation of my results in Proteus. In this regard, I thank Dr Sodja again for letting me pick his brain whenever I faced a bottleneck in the analysis. On that note, special thanks to Dr Christos Kassapoglou for the 'five-minute brainstorming meetings' on Friday mornings. I am also grateful to Dr D. H. Hodges (Georgia Institute of Technology) for responding promptly to my questions regarding papers co-authored by him.

I am indebted to Mr John Stals and Mr Ton Valk at TU Delft's Central International Office for helping me gain financial assistance from Schuurman Schimmel - Van Outeren Stichting and Stichting Peter de Konin respectively. Needless to say, I am also indebted to these organisations and deeply appreciative of the good work they do in supporting foreign students. Without their timely help, the completion of my graduate studies would not have been possible.

I am especially thankful to my friend Koushik Subramanian for his advice and support, both emotional and financial during the course of my graduate studies. Mentioned in Despatches: Richard J. Kruithof, for introducing me to the world of MATLAB, helping me clear Stability I, Composite Design and Analysis I and II and Non-Destructive Testing; not to mention letting me crash on his couch, Pranav D Sumanth and Shwetha Umesh for feeding the hungry; Thej Kiran, for being Thej.

Last but certainly not least, I am truly thankful to my parents and my younger brother for all the love and patience they have shown me. Without their cooperation and trust, I would not have been able to take the leap of faith required to move half-way across the world in pursuit of knowledge.

Himanshu Anand
Delft, April 2019

Abstract

Recent decades have seen the range of applications for aircraft expand to niches like weather monitoring, reconnaissance and satellite launch (Air Launch to Orbit, ALO). The requirements for such roles necessitate unconventional features like twin fuselages (in case of ALO mother ships) and very high aspect ratio wings (for long endurance missions). For conventional aircraft, aside from improving safety, the driving factors for new designs have always been increased efficiency and performance. The prevalent approach has been to reduce weight and induced drag by using higher aspect ratio wings. Consequently, newer designs are lighter, more flexible and closer the failure limit. Therefore, the interaction between flight loads and the airframe, i.e. aeroelasticity has become important for a safe design. High aspect ratio wings undergo large magnitude, low-strain deformations. An accurate understanding of their aeroelastic behaviour requires nonlinear analysis methods.

This thesis implements a reliable nonlinear aeroelastic analysis method in NASTRAN. The aeroelastic analysis modules in commercial finite-element analysis software are aerodynamically and structurally linear. At the same time, such software often has advanced nonlinear structural analysis capabilities. This thesis modifies and combines two approaches mentioned in literature. NASTRAN's aeroelastic module is used to obtain rigid aerodynamic loads and its nonlinear structural module to obtain structural deformations. For a given angle of attack, altitude and airspeed a wing is analysed iteratively until the rigid air loads and structural deformations for successive iterations converge. The nonlinear structural module is used to obtain pre-stressed structural modes for this converged condition. These modes are then used in flutter analysis.

An idealised HARW with arbitrary properties is analysed using this method and using TU Delft's in-house aeroelastic optimisation software: Proteus. Static aeroelastic deformations and flutter analysis results are compared for validation. Following this, the results of the linear and nonlinear aeroelastic analysis are compared. It is shown that linear analysis over-predicts the deformation in flexible wings and that the inclusion of pre-stress changes the damping of critical flutter modes; thereby changing the flutter point for the wing. For the test case analysed in this thesis, the inclusion of geometric nonlinearity and follower force effects resulted in large changes in the flutter speed with change in the angle of attack. In this way, the thesis successfully implements a nonlinear aeroelastic analysis method which can be used to improve aircraft designs during the preliminary stage.

Contents

Nomenclature

AAW	Active Aeroelastic Wing(s)
ACF(s)	Aerodynamic Correction Factor(s)
AIC(s)	Aerodynamic Influence Coefficient(s)
ALO	Air Launch to Orbit
AOA	Angle of Attack
AR	Aspect Ratio
BFF	Body Freedom Flutter
BWB	Blended Wing Body Configuration
BL	Boundary Layer
DLM	Doublet Lattice Method
DOF(s)	Degree(s) of Freedom
EOM(s)	Equation(s) of Motion
ESL	Equivalent Static Load
FCS	Flight Control System
FEA	Finite Element Analysis
FEM	Finite Element Model/Method
HALE	High Altitude Long Endurance
HAR	High Aspect Ratio
HARW	High Aspect Ratio Winged/Wings
HSCT	High Speed Civil Transport
JWC	Joined Wing Configuration
LE,TE	Leading Edge, Trailing Edge
MDS	Multibody Dynamic Simulation
NSS	Navier-Stokes Solver
ODE(s)	Ordinary Differential Equation(s)
RANS	Reynolds Averaged Navier-Stokes Solver
RBM	Rigid Body Mode/Motion
RLV	Reusable Launch Vehicle
ROM(s)	Reduced Order Model(s)
ROMM	Reduced Order Modelling Method
SIFS	Shock Induced Flow Separation
SL1	Scaled Composites LLC's StratoLaunch aircraft
SST	Supersonic Transport
TBW	Truss Braced Wing
TDT	Transonic Dynamics Tunnel (a NASA facility)
UAV(s)	Unmanned Aerial Vehicle(s)
VLM	Vortex Lattice Method
WTM	Wind Tunnel Model

1

Introduction

1.1. Motivation

Aeroelasticity investigates the interaction between aerodynamic, structural and inertial forces acting on an aircraft. Unlike the classical approach, where aerodynamic and structural analyses are separated, aeroelasticity considers deformations due to aerodynamic pressure. These deformations change the aerodynamic shape of the aircraft, altering the pressures acting on it. This continues until equilibrium. The earliest aeroplanes were quite flexible. Control surface flutter and divergence were frequently encountered aeroelastic phenomena around World War I. But the all-metal monoplanes which succeeded them deformed very little within their flight envelope. Aeroelasticity re-manifested as a problem towards the end of the second World War, when aircraft began to fly at speeds at which the compressibility of airflow posed a serious danger.

The field of aerospace engineering has continued to advance over the last century, with more capable powerplants and stronger, lighter materials becoming available. This has been accompanied by a constant demand for improved performance and efficiency. To meet this demand, new aircraft were and are being designed to operate closer to their failure limit. For large aircraft, like commercial airliners, the main objective is lowering operating costs by lowering fuel consumption. The prevalent approach to improve fuel efficiency has been to reduce weight and induced drag. The easiest way to reduce induced drag is to increase the aspect ratio (AR) of wings, to increase the lift. This has resulted in wings and fuselages becoming increasingly slender and flexible, ("Fig. 30 Wing aspect-ratio of airliners at year of introduction" [45]). Lighter, more flexible aircraft experience higher deformation due to aerodynamic loads. This makes aeroelastic considerations crucial for a safe design.

The range of applications for aircraft has continued to expand over the decades. Aircraft are being designed and built for ultra long reconnaissance and weather monitoring missions, to launch satellites from the upper atmosphere, to carry more passengers or heavier payloads. These new aircraft often have features that may be considered unconventional. This has been a common trend in the history of aviation. In each era, unconventional designs are tested to meet certain application requirements and some of these go on to become the norm. A good example of this is the B-47 Stratojet bomber. Its swept wings and cantilevered engine pods were considered radical for its time. But this design has served as a template for almost all the airliners in service today [70]. The word 'unconventional' can

have different meanings for different aspects of aircraft design. For instance, fly-by-wire control systems were unconventional until they came into widespread use. The original 'Jumbo Jet', the Boeing 747, the Airbus A-380 and the Boeing 787 Dreamliner are in widespread service today. But due to their size and the structural design required to make that size viable, they would've been considered unconventional in the early days of civil aviation. The air-launch-to-orbit (ALO) platform StratoLaunch is unconventional both in terms of its size (the largest aircraft ever built) and morphology (twin fuselages).

Unconventional aircraft designs are likely to experience flight and load regimes which leads to non-linear behaviour. That is, the relation between a cause and its effect is not linear. This nonlinearity can be structural, aerodynamic or control system related. Aerodynamic nonlinearities include shock, flow separation, effects of turbulent or compressible flow. Structural nonlinearities can be due to large deformation or loads beyond a structure's linear elastic limit. Such behaviour cannot be satisfactorily analysed by conventional methods. The accurate prediction of aircraft behaviour requires the inclusion of the relevant nonlinearities in the analysis.

The most common unconventional feature found in newer aircraft is, as mentioned above, high aspect ratio (HAR) wings. HAR wings have low stiffness because increasing stiffness will add weight and negate the advantage gained by additional lift. As a result, they exhibit large-magnitude, low-strain deformations (i.e. geometric nonlinearities). Stresses in HAR wings can easily cross the linear elastic limit under normal operating conditions, leading to nonlinear material behaviour. Accounting for these effects in the aeroelastic analysis is of relevance to the current research in the field.

1.2. Research Question, Aims and Objectives

Most of the literature on nonlinear aeroelastic analysis describes customised, stand-alone software. This thesis aims to develop a reliable nonlinear aeroelastic analysis method using commercially available tools and validate it using results from literature or using other existing nonlinear aeroelastic analysis tools. Such a method can help improve the design process of aircraft, especially those exhibiting nonlinear behaviour, by allowing the effect of these nonlinearities on the aircraft characteristics to be included in the early stages of design itself. From the survey of literature covered in Chapter 2, the most common reason for inaccuracy in the analyses of such aircraft is the exclusion of geometric nonlinearities and the follower characteristic of aerodynamic loads. With these points in mind, the research questions have been formulated as follows:

Main question: How can geometrically nonlinear aeroelastic behaviour of high aspect ratio wings be investigated reliably and efficiently using commercial solvers?

Sub questions:

1. How to model a HARW aircraft for nonlinear aeroelastic analysis in NASTRAN?
   (a) Which features to exclude/include in the structural, aerodynamic models?
   (b) With respect to linear aeroelastic analysis, to what extent would including geometric nonlinearities and follower force effects improve the results?[1]
   (c) What modifications are needed to standard NASTRAN elements and modules for investigating non-linear flutter in such an aircraft?
2. How to verify the accuracy of results in the absence of experimental data?

[1] Nonlinear material behaviour was not included due to time constraints.

2

Literature Review

The literature on nonlinear aeroelastic analysis and related topics was studied extensively to determine whether the aims of the thesis are relevant, realistic and non-redundant with respect to current research. The review also provided an outline of the modelling and analysis methodology. Any aeroelastic analysis requires a structural model, an aerodynamic model and a means of transferring information (loads, displacements) between them. Hence, the literature reviewed is grouped into:

- Survey of aeroelasticity and its relevant sub-disciplines
- Structural modelling for nonlinear aeroelastic analysis
- Aerodynamic modelling and aero-structural interpolation for nonlinear aeroelastic analysis
- Flutter analysis of aircraft with HAR wings (HARW) or an unconventional design.

2.1. Survey Papers

Survey papers present concise and verified information on noteworthy research in a field, gathered from multiple sources. A study of such papers shows that the majority of aeroelastic research can be grouped into two categories. One body of work seeks to improve aircraft performance by exploiting aeroelasticity. The second seeks to predict aircraft behaviour accurately in order to reduce the need for expensive and risky flight tests. Some survey papers also provide important insights specific to the design, analysis and behaviour of HAR wings.

Classic works like Collar [34] and Ashley [6] illustrate the vastness of the field of aeroelasticity. In his 1946 paper, Collar [34] discusses the importance of including flexibility in flight dynamic analysis and presents his famous “Collar’s triangle of forces” (figures 1-3, [34]), which defines aeroelasticity in a nutshell. He also states that including rigid body motion (RBM) of an aircraft in aeroelastic analysis is necessary to capture phenomena like body freedom flutter (BFF) and antisymmetric flutter modes. This point is also stressed in well-known textbooks on aeroelasticity, such as Bisplinghoff et al. [12].

Livne and Weisshaar [70] summarize a century’s worth of work on the development of unconventional aircraft and the resulting advances in aerospace engineering. The problems encountered during

the development of some notable aircraft are discussed in detail, e.g. aileron reversal in the XB-47 and BFF in Dick Rutan's Voyager. It is shown how the experience gained from solving these problems can improve the design and analysis of future aircraft. Emphasis is placed on the interaction of RBM and elastic natural modes in flexible aircraft. The importance of structural, aerodynamic and control nonlinearities in the analysis of new or unfamiliar aircraft designs is stressed.

Ashley [6, 7] outlines the salient research problems and advances in fixed-wing aeroelasticity up to 1986. Friedmann [46] lists significant developments in aeroservoelasticity, rotary wing aeroelasticity and experimental aeroelasticity between 1978 and 1999. Livne [69] explains the origin of various aeroelastic sub-disciplines and lists the significant developments up to 2003. Dowell [39], Dowell et al. [40] survey the field of nonlinear aeroelasticity and classify nonlinearities as either structural or aerodynamic. Afonso et al. [2] provide a more recent state-of-the-art survey on nonlinear aeroelastic research specific to HARWs. Geometric and material nonlinearities, flow separation at high angles of attack (AOA) and control effectiveness are identified as the most relevant nonlinearities for HARWs, because of the high deformations experienced by them. Like in [70] and [69], the importance of coupling between RBM and structural natural frequencies is emphasized. Work by M. J. Patil, D. H. Hodges and C. E. S. Cesnik (PHC) [83, 86] and Su and Cesnik [111] is cited to show how flutter speed and stability is affected by the stress state (i.e. deformation) of the wing. Commercially available finite elements are stated as the best option for nonlinear analysis.

Survey papers also describe a 3-tiered approach as being the norm for aeroelastic design, analysis and testing in the industry [2, 46, 69]. Preliminary design and analysis involve a large number of configurations and load cases. It uses low-fidelity 'stick' structural models coupled to linearised potential-flow based "panel code" aerodynamic models. Mid-level design uses more detailed structural models with aerodynamic models capable of capturing compressibility and viscous effects. Finally, computationally expensive, hi-fidelity structural and flow models are used during detailed design and certification stages to analyse critical load cases. Efforts are being made to reduce the computational cost of hi-fidelity flow models in order to improve the accuracy of preliminary and mid-level design. This is why computational aeroelasticity (where aerodynamic loads are obtained from CFD, not linearised panel codes or wind tunnel tests) is emerging as an area of interest [69]. Schuster et al. [101] and Edwards [42] present a survey of work done in this field. As of now, panel codes in general and the Doublet Lattice Method [3] (DLM) in particular are the most commonly used aerodynamic models for aeroelastic analysis [2]. Though they are limited to incompressible and inviscid flow, the time-advantage they offer outweighs their limitations. CFD and full Navier-Stokes Solver (NSS) based aeroelastic analysis will not become the norm for quite some time [69].

To summarize, nonlinear aeroelastic analysis is an important area of research. Work is being done to include different types of nonlinearities in analysis at a low computational cost and accurately predict the real-world behaviour of an aeroplane. Developing an efficient and reasonably accurate method for the nonlinear aeroelastic analysis is certainly relevant w.r.t the current state of the art of the field.

2.2. Structural Modelling

Linear analysis is limited to small deformations, where the assumption of a linear relationship between load and strain is valid. But real flight conditions often cross the limits of the 'small displacement' assumption. The rule of the thumb is, for a fixed number of elements, the number and type of nonlinearities included in the analysis determine how close the results are to the actual behaviour of an aircraft [17, 33].

There is a consensus in literature about geometric nonlinearity, material nonlinearity and the interaction between RBM and elastic modes as being the most relevant structural nonlinearities for HAR wings [2, 34, 69, 70]. The analysis of this thesis is currently limited to cantilevered wings and cannot include RBM-elastic interactions. Geometric nonlinearity manifests as low strain, large magnitude deformations [59, 109, 110]. Even in normal operating conditions, these deformations are large enough to alter the aerodynamic shape and in turn change the aeroelastic characteristics of the aircraft [86, 110]. In 'extra-normal' cases, a gust or a manoeuvre for instance, these deformations can exceed linear elastic limits and induce nonlinear material behaviour. Radcliffe and Cesnik [90] model material nonlinearity in hinged wings by using bilinear stiffness. Su [110] uses this approach to analyse skin wrinkling in an ultra-light, flexible flying wing.

To understand the best way to model HAR wings, about a 90 papers related to nonlinear aeroelastic and nonlinear structural dynamic analysis were reviewed. Approximately one-third of these papers proposed new formulations for nonlinear modelling and analysis. The rest used some of these new methods and other existing formulations to analyse conventional HARW aircraft, HAR Joined Wing Configurations (JWC), HAR Blended Wing Body (BWB) aircraft and composite rotor blades (Table 2.1). A majority of the papers chose to idealise HAR wings using beam elements. A few, like Harmin and Cooper [52], used 2-D shell elements instead. This simplified representation is necessary to make the analysis of a large number of load cases computationally viable. To ensure the accuracy, such models derive their stiffness and mass-distribution from the results of finite element (FE) analysis of detailed FE models or the dynamic testing of physical models. Singh and Nichols [107] describe a prevalent method for deriving an equivalent 1-D beam model from a 3-D FE model. The mass distribution in these 'reduced' models is often simulated by the 'barbell approach', where lumped masses are distributed about the beam axis and connected to structural nodes by rigid elements [4, 33].

Analysed Object	**Ref. No.**
HAR wings or HARW aircraft	[1, 4, 5, 8, 18, 19, 28, 31, 47, 52, 59, 64, 65, 73, 74, 76, 77, 83, 85, 86, 96, 97, 100, 105, 113, 115, 116, 121]
HAR joined wing aircraft	[11, 13, 22, 36–38, 63, 67, 87, 108, 117]
HAR blended wing body aircraft	[10, 62, 75, 82, 94]
Composite rotor blades or wing boxes	[9, 23–26, 29, 32, 58, 91, 92, 104]

Table 2.1: A summary of the type of aircraft analysed in the literature reviewed

Even if one has narrowed down the choice for idealising a wing to a beam, the formulations available are legion. However, as seen in Table 2.2, three types of beam models are in widespread use: displacement-based, strain-based and intrinsic. Displacement-based (or stiffness) formulations, as the name suggests, have displacements and rotations as the independent variable in the equations of motion (EOMs). Most commercial FEA software use displacement based models [79, 96]. Strain-based models use strains and curvatures directly in the EOMs as independent variables. This makes such models better at capturing RBM, avoiding shear locking and dealing with arbitrary loads and motions [79, 96]. Intrinsic models have no displacement or rotation variables in the EOM, i.e. deformation is 'intrinsic' to the equations. Stress resultants at the beam reference axis, non-dimensional strains and velocities are used as independent variables.

A significant portion of the papers reviewed cited work done by PHC on the aeroelastic analysis of a High Altitude Long Endurance (HALE) drone [80, 82, 83, 85, 86]. They also cited the analysis of actively controlled HAR wings by Brown [15] and Cesnik and Brown [21, 22] and the modelling of composite

Model/formulation	Ref. No.
Commercial FE (e.g. NASTRAN) i.e. displacement-based	[1, 4, 8, 10, 11, 13, 36, 37, 41, 47, 52, 58, 62, 74–76, 87, 91, 92, 94, 96, 97, 117]
Multi-body dynamic simulation (MDS)	[9, 18, 19, 38, 64, 65, 90, 125]
Intrinsic beam model by Hodges and Dowell [57] and Hodges [55, 56] with VABS [23]	[5, 24–26, 29, 31, 32, 73, 77, 82, 83, 85, 86, 104, 113, 115, 116, 121]
Custom, strain-based FE	[15, 21, 22, 27, 28, 110–114]

Table 2.2: Commonly used structural models for nonlinear aeroelastic analysis

rotor blades by Cesnik et al. [29, 30]. While Cesnik and Brown used a strain-based model, PHC used a mixed variation formulation developed by Hodges [55], based on geometrically exact, intrinsic EOMs for dynamics of moving beams. This model is most often used in conjunction with Variational-Asymptotic Beam Sectional Analysis (VABS) a tool developed by Cesnik and Hodges [23] for reducing 3-D slender structures to 1-D beams moving in 3-D. In effect, all the papers referring to PHC's work use some version of Hodges' [55] intrinsic model. Because intrinsic models use derived quantities directly as variables (stress as a derivative of force, strains and velocities as space and time derivatives of displacement), the overall order of the EOMs is reduced. This makes them robust and faster w.r.t stiffness or strain models [79]. However, they are not a standard feature in commercial FE software. Implementing a dynamic analysis using an intrinsic model would require extensive programming to define everything from the constitutive relations for the elements to the global dynamic EOMs.

As seen in Table 2.2, a small number of papers adapted the multi-body dynamic simulation (MDS) method to aeroelastic analysis. MDS is meant to study the motion of complex mechanisms. It models a system as a set of rigid bodies interconnected by kinematic and force constraints [103]. Elastic deformation is calculated internally for each body, using standard linear FEM [17]. Including structural nonlinearities requires using the finite segment [35][125] or finite volume[49] methods. Castellani et al. [17] compare the results of the nonlinear aeroelastic trim analysis of PHC's HALE drone [86] using MDS and FEM. Both methods are found to have similar computational cost and accuracy. Given that using MDS would not offer a significant advantage in computational efficiency or accuracy and the fact that FEM software is more readily available, this avenue will not be pursued.

A majority of the papers used displacement-based beam elements from commercial FEA software (mostly NASTRAN). These were either modified to include nonlinearities like anisotropy [92], or could model geometric nonlinear behaviour by default. Literature comparing the capabilities of intrinsic and stiffness models were studied ([59, 79]) and it was concluded that any increase in accuracy and speed gained by using an intrinsic model did not justify the extensive set-up effort involved. NASTRAN is a rigorously verified FEA solver which has been in widespread use for decades. The nonlinear beam elements available therein should be reasonably accurate for nonlinear aeroelastic analysis. If required, additional nonlinearities can be added to the NASTRAN beam using Direct Matrix Abstraction Program (DMAP), NASTRAN's internal programming language. For instance, Mei and Rogers [72] used DMAP to modify the linear beam element and subroutines to include geometric nonlinearities in NASTRAN's standard linear vibration analysis module. Thus, the nonlinear beam element from NASTRAN is chosen for the analysis in this thesis.

2.3. Aerodynamic Modelling

The core of any aerodynamic or flow model is an equation or a set of equations that quantify the flow of air and its interaction with solid bodies. The 'superset' of all flow models consists of five coupled,

nonlinear partial differential equations (PDE); collectively referred to as the Navier-Stokes equations (NSE). The NSE PDE describe continuity and the conservation of mass, momentum and energy in three dimensions for the motion of a viscous, compressible fluid. They are used to describe flow over an incredible range of size, speed and complexity; from weather patterns to the flow through a pipe. Different assumptions are made to derive simplified versions of NSE; each being a flow model suited to a different application. Figure 2.1 shows the hierarchy of various flow models in relation to NSE. When any of these equations is applied to a realistic engineering problem, it has to be discretized (i.e. modelled) and solved numerically. These numerical representations are the 'aerodynamic models' referred to earlier. Existing models range from simple 2-D potential flow based to full NSS.

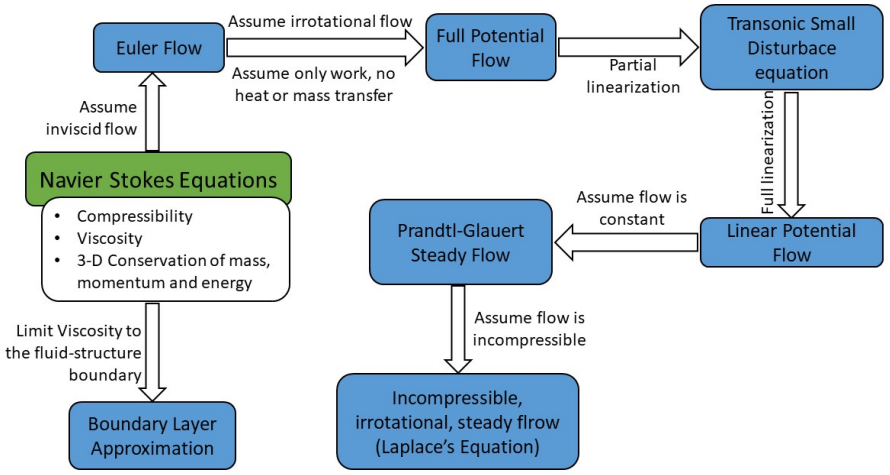

Figure 2.1: Aerodynamic flow models and their relation to Navier-Stokes Equation (adapted from "Figure 3.19: Models for unsteady aerodynamic flows" [60])

As stated in Section 2.1, simple models based on linear potential flow are used for preliminary design [69]. Panel codes, like VLM [54] and DLM [3] are the most widely used [2]. Detailed design and analysis uses intermediate complexity models capable of capturing compressibility and viscosity at a lower computational cost than full NSS models. These are often based on nonlinear potential flow or boundary layer (BL) approximation. NASA's CAP-TSD code, based on the transonic small disturbance (TSD) equation, is one such example. It was used by Silva and Bennett [106] to analyse the wind tunnel model (WTM) of NASA's active aeroelastic wing (AAW). Results from previous experiments in NASA's Transonic Dynamics Tunnel (TDT) were used to verify the accuracy of their analysis. Finally, the critical load cases are analysed using hi-fidelity full NSS or Euler flow models. A good example is the nonlinear aeroelastic analysis of a truss braced wing (TBW) by Bartels et al. [8]. DLM was used for low-fidelity analysis and FUN3D, a 3-D NSS code, was used for high-fidelity simulations. Another example of a hi-fidelity aerodynamic tool is CFL3D, used to analyse limit cycle oscillations in the B-1 bomber [53]. Such mid and hi-fidelity aerodynamic models are usually either proprietary or require extensive programming to deform the aerodynamic mesh in response to structural displacements.

Of the 60-odd papers in Table 2.2, only 3 used a nonlinear aerodynamic model [8, 10, 47]. The rest used panel codes. A panel code divides lifting surfaces into planar 'panels' and then into regular arrays of aerodynamic 'boxes'. The pressure at each box and its influence on the pressures at other boxes is taken together to calculate the lift distribution for the whole surface. Panel codes are based on linear potential flow theory and cannot capture compressibility and viscosity effects like flow separation, shock and drag. Despite these limitations, unless high angles of attack or high dynamic pressures (e.g. due to supersonic/transonic flight at sea level) are involved, linear panel codes are accurate and computationally cheap. As a result, they are the default aerodynamic modelling option in most

commercial aeroelastic analysis tools like NASTRAN [95].

Since this thesis is focused on low-fidelity analysis and ease of implementation is one of the criteria, the DLM aerodynamic model offered by NASTRAN will be used. However in [59], aside from proving the efficacy of the NASTRAN beam model, Cooper et al. also illustrate the limitations of using DLM for nonlinear aeroelastic analysis. The main source of inaccuracy is exclusion of the 'follower effect' in aerodynamic forces. Lift stays normal to a wing's surface as it deforms. But in panel codes, the lift force has a fixed vertical orientation in the global reference frame. At high AOA or high wing deformation, a significant portion of the lift force is ignored by the panel code, leading to inaccuracy in results [17, 59]. A nonlinear aeroelastic analysis method using DLM would have to account for these limitations.

2.4. Static Aeroelastic Analysis

Aeroelastic analysis combines the structural and aerodynamic models discussed in previous sections to form a combined system of EOMs. In this system, output from the aerodynamic model (load) is used as input for the structural model. Output from the structural model (displacements) is used as input for the aerodynamic model. If the flow conditions vary very slowly with time, inertial forces can be ignored and the problem is static aeroelastic. Else, it is dynamic aeroelastic. For simple systems like a 2-D aerofoil section (aka the typical section) free to plunge and pitch, the number of structural and aerodynamic DOFs is equal. So, transferring information between the two models (i.e. coupling them) is a straightforward process of writing the force and moment equilibrium equations for each of the two DOFs (equations 2.6-2.8, Hulsoff [60]):

$$\begin{aligned} \sum F_z = 0 &\Rightarrow m\ddot{h} + S_\theta \ddot{\theta} + K_h h + L = 0 \\ \sum M_{EA} = 0 &\Rightarrow S_\theta \ddot{h} + I_\theta \ddot{\theta} + K_\theta \theta - M_{EA} = 0 \end{aligned} \tag{2.1}$$

K_h, K_θ are the stiffness in the plunge and pitch DOFs respectively; L is the vertical lift force and M_{EA} is the moment due to lift about the pitch/elastic axis (EA); m, I_θ are the aerofoil's mass and moment of inertia about the EA; S_θ is the static moment about EA; h is the vertical displacement of the aerofoil and θ the twist deflection about the EA; $(\ddot{})$ represents acceleration. For complex systems, special interpolation functions and algorithms have to be used. But the basic principle is the same as Equation (2.1). The analysis methods and results from a few of the papers listed in Table 2.2 are discussed briefly in the following paragraphs.

Patil, Hodges and Cesnik have conducted low-order, hi-fidelity nonlinear static aeroelastic analysis of an HARW HALE drone [86] by coupling beam dynamic equations developed by Hodges [55] to a finite-state air loads model [88]. The results showed very strong dependence between wing bending modes and rigid flight dynamics as well as a loss in lift due to the wing deformations. This, in turn, increased the trim AOA needed for level flight at a certain speed. The flutter speed (V_f) was also shown to be dependent on the wing deformation, although in a counter intuitive fashion. As the air loads were increased gradually, there was a sharp increase in V_f when the air loads overcame the effects of gravity and the wing started bending up instead of drooping down. The V_f then reduced smoothly as the wing deformation increased. However, as the AOA (i.e. the air loads) crossed $4.5°$, the wing deformation increased the natural frequency of the critical flutter mode, leading to an increase in V_f instead of the further decrease expected. Su [110] used a integrated formulation similar to PHC, but with strain-based finite elements, to analyse nonlinear static and dynamic behaviour of four unconventional configurations. This formulation could capture the effects of localised skin buckling (wrinkling) and the contribution of a flexible fuselage and tail (i.e. a full, flexible aircraft). Four very flexible configurations were analysed and the effects of RBM-elastic coupling were captured.

The above examples all use custom formulations. However, several papers show the suitability of standard FE models for nonlinear aeroelastic analysis. Saltari et al. [97] couple NASTRAN's nonlinear structural module to an external VLM code and use it to achieve good accuracy in the nonlinear aeroelastic analysis of a flexible flying wing. Riso et al. [94] use the same method to analyse a very flexible BWB drone, successfully capturing RBM-elastic interaction in their results. Howcroft et al. [59] compared 5 different ways to analyse the same HARW model and discussed the pros and cons of each method. Two FE based methods (quasi-nonlinear and nonlinear iterative) which coupled NASTRAN's nonlinear structural solver to its linear aeroelastic solver were compared with two multi-body dynamic simulation methods and a method using intrinsic beam dynamics based on Hodges [55]. The ease of implementing a nonlinear analysis using FEA software is clearly demonstrated, along with the tendency of panel method based aerodynamic models to over predict lift at high AOA. Nevertheless, the paper shows that the nonlinear NASTRAN beam is adequate for nonlinear aeroelastic analysis.

The nonlinear iterative method described in [59] is used by Salman et al. [96] for nonlinear aeroelastic trim analysis of a passenger jet. Here, rigid air loads from NASTRAN's linear aeroelastic module (Sol 144) are exported to its nonlinear structural analysis module (Sol 106). Then, the nonlinear displacements are used to create a new rigid wing in Sol 144 to get a new set of air loads. The process is continued until the air loads and nonlinear displacements from successive iterations converge. The quasi-nonlinear method from [59] was originally used to analyse a scaled wind tunnel model of an aircraft with a very high aspect ratio, truss braced wing (TBW) by Coggin et al. [33] and Zhao et al. [124]. A full scale FE model of this TBW aircraft was also analysed using the same method by Allen et al. [4]. In this method, rigid air loads from the NASTRAN Flightloads (which uses VLM) exported to its nonlinear structural module. Modal analysis is carried out on the static nonlinear equilibrium state and these pre-stressed modes are exported to the linear flutter solution. The process is repeated till the flutter speed converges. The results captured an increase in flutter speed due to the rearward shift in the centre of pressure at transonic speeds. Transonic compressibility was captured in VLM by using CFD results to correct VLM output.

2.5. Flutter Analysis

Flutter is a dynamic aeroelastic instability. It occurs when a dynamic disturbing force overcomes the inherent structural damping of an aircraft and induces vibrations/oscillations with ever increasing amplitude/energy. Garrick and Reed III [48] provide a very thorough history of the study of flutter, starting with tail flutter in World War I bombers, until 1981. A good overview of the theory behind the current methods used for flutter analysis is provided by Rheinfurth and Swift [93]. Van Schoor and Von Flotow [119], Van Schoor et al. [120] analysed a very flexible, human-powered aircraft for flutter using modified finite element structural models coupled to simple 2-D strip aerodynamic models. Drela [41] modelled a complete flexible aircraft using connected nonlinear beams, coupled the model to a VLM aerodynamic model [54], added compressibility corrections and carried out nonlinear dynamic aeroelastic analysis as part of the preliminary design process. Drela's work resulted in the development of a nonlinear aeroelastic analysis tool, ASWING, and has often been cited as a benchmark. Tuzcu and Meirovitch [118] outlined the effects of flexibility and the changes that need to be made to the analysis methods for flexible aircraft.

About 45 papers on the flutter analysis of flexible and unconventional aircraft were studied. A quarter of them dealt with Body Freedom Flutter (BFF), a flutter mechanism particular to very flexible aircraft, where the pitch RBM motion of the fuselage couple with the low frequency, 'flat-wise' natural bending modes of the wings and induce flutter [16, 51, 71, 98, 99, 112]. Another quarter deal with flutter in HAR,

slender wings [14, 20, 61, 81, 84, 89].
Almost half of them (22 of 45) use linear, unsteady aerodynamic models coupled with nonlinear FE models and are limited to linear flutter analysis. Standard p-k or V-g methods are used. A brief description of the p-k method is provided in the next chapter. In another one-third of the papers, nonlinearity is included either by creating flight-dynamics-elasticity-integrated formulations or by using a transonic [43, 106] or dynamic stall aerodynamic model [61, 81]. However, this thesis uses the linear panel code (DLM) provided by NASTRAN. The nonlinearity in flutter analysis is included by an iterative process using MATLAB to import a nonlinear equilibrium stress state into NASTRAN's linear flutter analysis module (Chapter 3). In essence, this is a linear dynamic analysis about a nonlinear static equilibrium.

2.6. Conclusion

Aeroelastic analysis consists of determining aerodynamic forces acting on an aircraft, transforming them into structural forces, calculating the resulting structural deformations/displacements and transforming these into displacements of the aerodynamic grid. At each stage of the analysis, certain idealizations and assumptions are made. Each assumption takes the results farther away from the actual behaviour of the vehicle. Different degrees of simplification are accepted for different fidelity levels in analysis. The most commonly made assumption is that of linear behaviour.

The purpose of this thesis is three fold. First, the different nonlinearities that are excluded from traditional, preliminary stage aeroelastic analysis have to be identified and their effects on the results have to be evaluated. Second, a method of feasibly including critical nonlinear behaviour in preliminary analysis (which has to be fast and computationally cheap out of necessity) has to be determined. Third, the analysis method has to be validated and used to analyse a high aspect ratio wing.

The literature study has helped establish a path to completing the first two objectives of the thesis. First, it has identified geometric nonlinearities and follower force effects as having the greatest effect on the aeroelastic characteristics of slender wings. These phenomena can also be included in aeroelastic analysis with less effort than say, including the nonlinearities induced by the hinges for folding the wings of carrier-based naval aircraft [90]. Second, the exercise has highlighted the salient advantages and drawbacks of various nonlinear aeroelastic analysis methods described in published literature. The ensuing choice regarding the analysis method is discussed further in the next chapter.

3

Analysis

The literature review has helped narrow down the nonlinearities most relevant to aeroelastic behaviour and the prevalent methods for including them in aeroelastic analysis. The efficiency, reliability and capabilities of these methods, as well as the effort required, to set them up has been examined in some detail in the previous chapter. Based on these criteria, the nonlinear iterative method described by Coggin et al. [33], Salman et al. [96] and Castellani et al. [17] has been selected and adapted for the analyses to be carried out in this thesis. It has good agreement with other nonlinear aeroelastic analysis methods [59] and can be implemented in NASTRAN; which enhances its 'portability'. Using a well-established FEA solver also facilitates validation. This chapter describes underlying principles of the nonlinear iterative method, the modifications made to it and the process of applying it for the nonlinear aeroelastic analysis of a high aspect ratio wing.

3.1. Structural Modelling

In this thesis, a simple, rectangular wing with no sweep, taper or dihedral is analysed. The wing has a half-span (b) of $16m$, a constant chord of $1m$ and no control surfaces. The wing dimensions are based on the HALE wing analysed by PHC [86] since this example is most commonly found in literature. The wing has an aspect ratio of 32 and is expected to exhibit geometric nonlinear behaviour.

Length	$16m$
Cross section outer dimensions	$0.85m \times 0.12m$
Thickness, front and rear walls	$7.5mm$
Thickness, top and bottom walls	$5.0mm$
Young's modulus (E)	$72.0GPa$
Shear modulus (G)	$26.9GPa$
Mass density	$2767.99kg/m^3$

Table 3.1: Wing box properties

The wing box is assumed to be made of an isotropic material with a hollow rectangular cross-section shape. The thickness of the cross-section walls are selected to provide reasonable flexibility,

determined by measuring the wing tip deflection under self-weight. The wing box is idealised as a beam and modelled using NASTRAN's nonlinear beam element: CBEAM [66]. A simple convergence study shows 16 beam elements to provide good accuracy in results. The structural dimensions and material properties of the wing are listed in Table 3.1 (also see Figure 4.1). A closed, symmetric cross-section ensures that the centre of gravity, the shear centre and the elastic axis (EA) or the centre of twist are coincident. Mass density is removed as a material property. The weight per unit length, calculated from the cross-section dimensions is used to determine the magnitude of lumped masses distributed about the beam axis and connected to the structural nodes using rigid elements. Lumped mass elements (CONM2 [66]) of $14.784kg$ each are placed at $\pm 0.5m$ of each of the 17 structural nodes.

The CBEAM element chosen here is based on NASTRAN's linear beam element, CBAR, which is based on classical beam theory. In CBAR, plane cross-sections remain plane in the deformed condition. The neutral axis and the shear axis are coincident. The cross-section (and therefore the stiffness and mass properties) is constant over the beam length. In CBEAM, each of these restrictions is relaxed. CBEAM supports the arbitrary variation of cross-sectional mass distribution and stiffness. Therefore, wings with sweep, taper and non-uniform mass distribution can be analysed. Elastic-plastic material models are supported. However, modelling anisotropic behaviour is difficult. Shear relief (due to taper) and cross-sectional warping coefficients can be specified. These features make CBEAM a very good option for creating low-order models of HAR wings. The exact formulae used by CBEAM are standard, 3-D nonlinear structural mechanics expressions. They can be found in [68] and will not be reproduced here. However, the nonlinear static analysis procedure is summarised briefly below.

Nonlinear Structural Analysis

Geometric nonlinearities are analysed using a co-rotational, updated Lagrangian formulation in NASTRAN's nonlinear static analysis module: Sol 106. Large displacements are resolved into large RBM rotations and small deformations. The element coordinates are updated using the last converged state and used to calculate the deformation (updated Lagrangian formulation [68]). The linear force-displacement relation is:

$$\{F\} = [K]^L\{u\} \tag{3.1}$$

The linear stiffness matrix $[K]^L$ is a function of material properties and the undeformed geometry. It does not change as the structure deforms. This idealisation becomes inaccurate for large deformations. So, for a nonlinear problem Equation (3.1) changes to:

$$\{F\} = [K](u)\{u\} = \left\{[K]^L + [K]^d(u)\right\}\{u\} \tag{3.2}$$

$[K]^d$ is the geometric stiffness matrix, also known as the differential stiffness matrix. It depends on the deformed geometry which in turn depends on the applied loads. Additionally, the orientation of the force vector is not constant. It follows the deformation of the structure. So, an additional 'follower stiffness' component, $[K]^f$ is added to the stiffness matrix:

$$[K]^t = [K]^L + [K]^d + [K]^f \tag{3.3}$$

The vector of nodal forces $\{F\}$, obtained using $[K]^t$ and Equation (3.2) is not the same as the vector of applied loads (say, $\{P\}$). Equation (3.2) has to be solved iteratively. In each iteration, the 'residual error' between $\{F\}$ and $\{P\}$ is used to update $[K]^t$. At equilibrium (adapted from Equation (3.2.1), [68]):

$$\{F\}^n - \{P\} = \{R\}^n \to \{0\} \tag{3.4}$$

Here, n is the iteration number. Sol 106 (and most FE methods) divides the applied load into increments $\{\Delta P\}$. For each increment, $[K]^t$ is iteratively updated until $\{R\}$ is minimised [68]. The converged,

deformed state for one load increment is used as the initial condition for the next load increment [68]. Thus, the final converged solution has the cumulative loads from all increments, which totals to the applied load. Depending on how the load is divided into increments and on the scheme for updating $[K]^t$, the nonlinear analysis method can be full Newton-Raphson ($[K]^t$ updated each iteration), quasi-Newton ($[K]^t$ updated once per load increment) or modified Newton ($[K]^t$ updated after n iterations). All these methods are supported in Sol 106 [68].

Preloaded Nonlinear Modal Analysis

The natural modes of a structure are calculated by solving the following eigenvalue problem:

$$\left[\omega_0^2[M_{aa}] - [K]^L\right]\{\phi\}_0 = 0 \tag{3.5}$$

Here ω_0 is a natural frequency, $[M_{aa}]$ is the structural mass matrix and $\{\phi\}_0$ is the corresponding mode shape normalised using the amplitude of the vibration. The subscript ($_0$) indicates that the structure is not loaded.

After Sol 106 has converged, modal analysis can be conducted on the nonlinear equilibrium state. As explained by Mei and Rogers [72], $[K]^t$ replaces $[K]^L$ for nonlinear modal analysis (Equation (18), Mei and Rogers [72]). In Mei and Rogers [72]'s method, actual (not normalized) linear mode shapes are used as displacement to calculate $[K]^d$. The eigenvalue problem of Equation (3.5) is solved iteratively, with the mode shapes of each iteration being used to update $[K]^d$ for the next iteration, until the eigenvalues and vectors meet some convergence criteria. This process was later included in NASTRAN as a standard feature. Instead of the linear mode shapes, the converged deformed state of the structure is used to get the first estimate for $[K]^d$.

$$\omega^2[M_{aa}]\{\phi\}_n = [K]^t\{\phi\}_n \tag{3.6}$$

$$\{u\}_n = \{\sigma\}_{n-1}\{\phi\}_{n-1} \tag{3.7}$$

Equation 3.6 is solved iteratively until the mode shapes and frequencies converge. Here, $\{\phi\}_n, \{\sigma\}_n$ are estimates of the normalized eigenvectors and vibration amplitudes for iteration n, respectively. This captures the nonlinear effects of applied loads on the natural mode shapes of a structure.

3.2. Aerodynamic Modelling

The wing was modelled as a single, planar lifting surface using NASTRAN's internal aerodynamic model, the Doublet Lattice Method (DLM). The aerodynamic mesh consisted of 32 span wise boxes and 8 chord wise boxes.

DLM [3] is a panel method which models unsteady flows in the frequency domain. It is based on the linear potential flow equation (Equation (3.24), Hulsoff [60]):

$$\nabla^2\phi - M_\infty^2\frac{\partial^2\phi}{\partial x^2} - \frac{1}{a_\infty^2}\left[\frac{\partial^2\phi}{\partial t^2} + 2U_\infty\frac{\partial^2\phi}{\partial x \partial t}\right] = 0 \tag{3.8}$$

The subscript ($_\infty$) denotes 'free-stream' flow conditions. ∇^2 is the Laplacian; ϕ is the perturbation potential (perturbation velocity $v = \nabla\phi$). U is the flow speed and a is the speed of sound. For steady, incompressible flow, Equation (3.8) reduces to the Laplace equation ($\nabla^2\phi = 0$). Another widely used panel method, the vortex lattice method (VLM) by Hedman [54] is based on the Laplace equation.

In DLM, Equation (3.8) is expressed in terms of an 'acceleration potential'. The change in flow conditions is assumed to be harmonic and of small amplitude. Lifting surfaces are discretized into

regular arrays of trapezoidal boxes whose chord wise edges are parallel to the flow direction (Figure 3.1). The acceleration potential is assumed to be concentrated along a line of 'doublets', located at the quarter-chord line of each box. The normalwash (ratio of normal velocity over a surface to the free stream velocity) induced by each box is assumed to be proportional to the doublet strength for that box. The doublet strength varies from one box to another, but is uniform across the span of any single box. Downwash generated at one box contributes to the downwash generated at all other boxes. The total downwash at box i is given by (Equations (5) to (6) Albano and Rodden [3]):

$$\bar{w}_i = \sum_{j=1}^{n} \bar{w}_{i,j} = \sum_{j=1}^{n} D_{ij}\bar{p}_j \tag{3.9}$$

$\bar{w}_i$ is the total downwash at box i, $\bar{w}_{i,j}$ is the component of $\bar{w}_i$ due the doublet strength of box j. The matrix D_{ij} connects the pressure coefficient ($\bar{p}_j$) to the downwash at each box.

$$[D_{ij}] = [A_{ij}]^{-1} = \frac{\pi}{8}\left[\Delta x_j \cos\lambda_j \int_{l_j} K.d\mu\right] \tag{3.10}$$

K is the "subsonic kernel function" [3] a large analytical expression that is a function of the displacement of a box, the Mach number (M), the flow velocity (U) and the angular frequency (ω); $\Delta x_j, \lambda_j$ are the chord width and sweep at quarter-chord for box j; $d\mu$ is an infinitesimal length along the doublet line and l_j is the doublet line length for box j.

$$p_i = q\bar{p}_i = \sum_{j=1}^{n} \bar{p}_{i,j} = \sum_{j=1}^{n} [A_{ij}]\bar{w}_j \tag{3.11}$$

Pressure coefficients $\bar{p}_i$ are dimension less quantities, which when multiplied by the dynamic pressure q, give the pressure at the mid-span, three-quarter chord point of a box. Like $\bar{w}_{i,j}$, $\bar{p}_{i,j}$ is the component of $\bar{p}_i$ due to the pressure contribution from box j.

$$\bar{Q}_{ij} = \frac{1}{b_r^2 s_r} \sum_{k=1}^{n} h_k^i \bar{p}_k^j S_k \tag{3.12}$$

Q_{ij} is the generalised aerodynamic force (GAF) coefficient; b_r, s_r are the reference half-chord and half-span of the wing respectively, S_k is the area, h_k^i the deflection in (oscillatory) mode i and $\bar{p}_k^j$ the pressure coefficient in mode j for box k.

NASTRAN uses a version of these equations [95] which allow corrections to the downwash based on experimental data. This way, the effects of camber, twist, initial incidence etc. can be included. The matrix of aerodynamic forces is defined as (adapted from Equations (2-3) and (2-4), [95]):

$$\{P_k\} = [S_{kj}]\{f_j\} = q[Q]_{kk}\{u_k\} \tag{3.13}$$

Here, $[S_{kj}]$ is an integration matrix, $[Q_{kk}]$ is the influence coefficient matrix for aerodynamic forces (analogous to Q_{ij} from Equation (3.12)). $\{u_k\}$ is the matrix of aerodynamic displacements with $k = \omega b/U$ being the reduced frequency. Using the actual pressure distribution, $\{f_j\}^{ex}$, measured at a reference angle of incidence; the downwash matrix $\{w_j\}$ can be modified as follows (adapted from Equations (2-1), (2-2) and (2-20), [95]):

$$\{w_j\}^{ex} = [A_{jj}]\{f_j\}^{ex}/q \tag{3.14}$$

$$\{w_j\} = \{w_j\}^{th} + \{w_j\}^{ex} \tag{3.15}$$

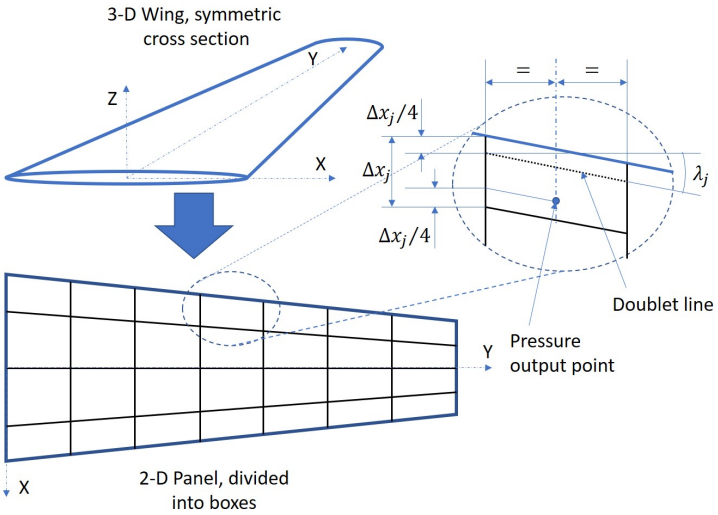

Figure 3.1: Discretization of a wing in DLM

The superscripts $(^{th})$ and $(^{ex})$ indicate theoretical and experimental values respectively. The subscript $(_j)$ indicates a box number. $[A_{jj}]$ is the aerodynamic influence coefficient (AIC) matrix for pressure. In effect, Equation (3.15) reorients the normal vectors for the boxes in a lifting panel. In NASTRAN this is done using a matrix which lists the local AOA for each box (DMI W2GJ card, [95]). Instead of describing the cambered shape of the wing, the same matrix can be used to import twist deformations from the nonlinear structural module as well. The GAF matrix $[Q]_{kk}$ can also be modified by multiplication with a correction factor matrix $[CF]$ derived from experimental data [50] or CFD simulations [78]. Equation (3.13) can then be rewritten as (adapted from equation (2-21), [95]):

$$P_k = q[CF][Q_{kk}]\{u_k\} + [S_{kj}]\{f_j\}^{ex} \tag{3.16}$$

The matrix $[CF]$ can be used to include compressibility effects like the aft-shift in the centre of pressure at transonic speeds [4] and thus expand the dynamic pressure range over which panel method results are reliable.

3.3. Nonlinear Static Aeroelastic Analysis

For static aeroelastic analysis, NASTRAN uses “splines” [95], a class of customised interpolation functions based on beam and plate theories, to transfer loads and deformations between the structural and aerodynamic models. Structural displacements ($\{u_g\}$) and aerodynamic loads ($\{P_k\}$) are treated as the independent variables (Equations (2-22), (2-25) and (2-64) [95]):

$$\{u_k\} = [G_{kg}]\{u_g\} \tag{3.17}$$

$$\{F_g\} = [G_{kg}]^T\{P_k\} \tag{3.18}$$

$$[Q_{aa}] = [G_{ka}]^T[Q_{kk}][G_{ka}] \tag{3.19}$$

Here $[G_{kg}], [G_{ka}]$ are interpolation matrices and $[Q_{aa}]$ is an AIC matrix relating structural deformation to structural forces. The EOM for static aeroelastic analysis is (adapted from equation (2-66), [95]):

$$\left[[K]^L - q[Q_{aa}]\right]\{u_g\} + [M_{aa}]\{\ddot{U}_g\} = q[Q_{ax}]\{u_x\} + \{P_a\} \tag{3.20}$$

Here $\{\ddot{U}_g\}$ is the vector of structural accelerations and $\{u_x\}$ is the displacement vector for aerodynamic RBM (roll, pitch, control surface deflections etc.). $[Q_{ax}]$ is an AIC, interpolated like $[Q_{aa}]$, providing

forces at structural nodes due to aerodynamic RBM displacements. $\{P_a\}$ are extra applied forces, like those due to landing or control surface deflection. For simplicity, the current analysis does not consider RBM and the wing model has no control surfaces. So, Equation (3.20) reduces to:

$$\left[[K]^L - q[Q_{aa}]\right]\{u_g\} = 0 \tag{3.21}$$

Linear static aeroelastic analysis is done using NASTRAN's Sol 144 module. Aerodynamic loads are calculated using DLM (Equation (3.16)). Spline functions transfer these loads onto the structural model and linear FEM calculates structural displacements. These displacements are transferred to the aerodynamic mesh and the air-loads are recalculated. The process is repeated until equilibrium in Equation (3.20) is satisfied [95].

For nonlinear static aeroelastic analysis, the structural model in Sol 144 is made rigid. The matrix $\{F_g\}$ now represents rigid air loads interpolated on to the structural nodes. These loads are exported to Sol 106 and the original flexible structure is analysed using nonlinear static analysis. By exporting the interpolated loads to Sol 106, the linear stiffness matrix ($[K]^L$) is replaced by a tangential stiffness matrix $[K]^t$ (Equation (3.3)) and the structural displacements $\{u_g\}$ become nonlinear $\{u_g\}_{NL}$.

After Sol 106 converges, $\{u_g\}_{NL}$ is used to update the rigid wing geometry in Sol 144. Multiple lifting panels are used, so as to fit the deformed geometry more closely. Nonlinear displacements are used to reorient the panels in three dimensions and rotations are used to update the initial incidence in the panel boxes ($\{w_j\}^{ex}$ in Equation (3.15)). This transfers displacements due to geometric nonlinearities to the aerodynamic model and approximates the 'follower' nature of aerodynamic forces. Sol 144 is run again to obtain a new set of rigid air loads, which is then exported to Sol 106. The process is repeated until $\{u_g\}_{NL}$ converges. In effect, this 'decouples' the structural and aerodynamic components of Equation (3.21). Let n denote one iteration of the Sol 144-Sol 106 loop. Then we have:

$$\{F_g\}_n - [K]_n^t\{u_g\}_{NL}^n = \{0\} \tag{3.22}$$

$$\{P_k\}_n = q[Q_{kk}][G_{kg}]\{u_g\}_{NL}^n \tag{3.23}$$

$$\{F_g\}_{n+1} = [G_{kg}]^T\{P_k\}_n \tag{3.24}$$

The aim is to achieve an equilibrium where two convergence criteria are met. First, the nonlinear displacements from two consecutive Sol 106 iterations have to be within 0.1% of each other. Second, the bending moment due to the total lift force at the wing root for two successive Sol 144 iterations are within 0.01% of each other. By using both force and displacement controls, chances of a false positive are reduced and the reliability of results improves.

3.4. Flutter Analysis

Flutter is the divergent oscillatory response of an aircraft to excitation by aerodynamic loads. Flutter analysis tries to find the boundary of flight conditions which produce self-sustained, constant amplitude oscillations in a wing or an aircraft. Within this boundary, oscillations are damped (i.e. reducing in amplitude). Beyond this boundary, oscillations grow in amplitude until a catastrophic failure occurs. Since flutter involves harmonic motion, most flutter analysis methods use approaches similar to structural vibration analysis [95]. The state of the structure is expressed as a function of its natural modes [102]. That is, its mass, stiffness, geometry and deformations are generalised (made dimensionless) using its natural mode shapes and frequencies.

It is known that motion at the flutter boundary is a constant amplitude oscillation. So, aerodynamic loads are also assumed to harmonic. This assumption is accurate only at the flutter boundary. As

a result flutter analysis solutions are also exact only at the flutter boundary. Aerodynamic forces are modified in various ways and added to the structural modes to find 'aeroelastic modes'. If the eigenvalues for an aeroelastic mode is complex and positive, it indicates flutter [12]. The method in which aerodynamic contribution is included in the eigenvalue problem distinguishes one flutter method from another. The aeroelastic EOM used in flutter analysis is (Equation (9.1), Hulsoff [60]):

$$[\hat{M}_{aa}]\{\ddot{q}_m\} + [\hat{D}]\{\dot{q}_m\} + [\hat{K}]\{q_m\} = \{Q_A\} \tag{3.25}$$

$\{q_m\} = \{\bar{q}_m\}e^{pt}$ are modal coordinates, not to be confused with the dynamic pressure q, ($\hat{}$) indicates that a matrix has been generalised. $[\hat{M}_{aa}], [\hat{D}], [\hat{K}]$ are then, the modal (i.e. generalised) structural mass, modal structural damping and modal structural stiffness matrices respectively; $\{Q_A\}$ is the matrix of generalised aerodynamic forces. In NASTRAN, instead of $\{Q_A\}$, a matrix of generalised aerodynamic force coefficients ($[Q_{hh}]$) is derived so that:

$$\{Q_A\} = q[Q_{hh}]\{q_m\} \tag{3.26}$$

$[Q_{hh}]$ is derived by modal reduction of $[Q_{kk}]$ [95] after it has been interpolated onto the structural nodes using Equation (3.19). It is a complex matrix and a function of the Mach number (M) and the reduced frequency of oscillatory motion, k. Calculating it is computationally expensive. So, for efficiency, NASTRAN pre-calculates $\{Q_{hh}\}$ at user defined (M, k) values. The matrix is interpolated to the k values being used in flutter analysis.

NASTRAN's linear flutter analysis module (Sol 145) offers three methods for flutter analysis: K, KE and PK [95]. In the K-method, $\{Q_A\}$ is expressed as 'aerodynamic mass' and added to the modal mass matrix $[\hat{M}_{aa}]$. In the PK method, real ($[Q_{hh}]^R$) and imaginary ($[Q_{hh}]^I$) parts of $\{Q_{hh}\}$ are added to $[\hat{D}]$ and $[\hat{K}]$ as modal aerodynamic damping and stiffness terms. This gives an equation in terms of the complex eigenvalue p and the reduced frequency k, (hence the name: p-k). For the analysis done in this thesis, the PK method was selected because its results are easier to interpret. In the PK method, each flutter summary table is for a single flutter mode whereas, in the K method, a mode has to be traced across multiple tables. This makes automated creation of flutter plots using PK flutter summary tables more feasible than with K flutter tables. The equation for PK flutter analysis is (adapted from Equation (2-128), [95]):

$$\left[[\hat{M}_{aa}]p^2 + \left([\hat{D}] - \frac{1}{4}\frac{\rho\bar{c}U}{k}[Q_{hh}]^I\right)p + \left([\hat{K}] - \frac{\rho U^2}{2}[Q_{hh}]^R\right)\right]\{q_m\} = 0 \tag{3.27}$$

$$p = \omega(\gamma \pm i) \tag{3.28}$$

Here $\bar{c}$ is the reference chord and ρ is the air density; $\gamma/2 = g$, the structural damping coefficient used in $V - g$ plots. The solution proceeds one flutter mode and one velocity at a time. At zero velocity, flutter modes are the same as structural mode shapes. So, the initial value of k is calculated using natural frequency (in radians) of the corresponding structural mode; p is assumed to be completely imaginary ($p_1 = \pm\omega i$). Equation (3.27) is solved iteratively until the value of p converges. Then the velocity is increased and the process is repeated. After the full velocity range is covered for one mode, the process is repeated for the next flutter mode. The converged g, ω values for different velocities in each mode are tabulated and plotted against the velocity (U) to locate the flutter point. At the flutter point, the g becomes positive, indicating oscillations of increasing amplitude.

Structural nonlinearities can be included in linear flutter analysis by using preloaded modes instead of linear modes for modal reduction of matrices in Equation (3.25). After the nonlinear static aeroelastic analysis converges, Sol 106 is used to calculate preloaded natural modes (Section 3.1). The converged nonlinear static solution (with preloaded modes) can be directly imported into Sol 145. This would

include the effects of geometric nonlinearities in the generalised aerodynamic and structural matrices. It also ensures that the stiffness matrix used is $[K]^t$ and not $[K]^L$.

For linear flutter analysis, Sol 145 needs to be run a single time to analyse all flutter modes at all velocities of interest. However, the nonlinear equilibrium state depends on the aerodynamic loads at a certain velocity. For small changes in velocity, the overall stress state of the wing might not change appreciably. But the $[K]^t$ for $U = 30m/s$ will be different from that for $U = 90m/s$. Therefore, multiple Sol 145 analyses are required. For each analysis, the converged stress state and preloaded modes from Sol 106 are imported and used for modal reduction. The g, ω values from all Sol 145 output files are retrieved, collated and plotted to create a $V - g$ plot.

3.5. Analysis Set-up

NASTRAN uses text files with the extension $.bdf$ as input. The type of analysis to be carried out, the output required and sets for analysis parameters, loads and boundary conditions are specified in the 'executive control' and 'case control' sections at the beginning of the file. This is followed by a 'bulk data' section where the finite element model and the actual loads, boundary conditions and analysis parameters are defined. The output generated is in the form of formatted tables, stored in text files with the extension $.f06$. A MATLAB program was written to read the relevant output from $.f06$ files, create $.bdf$ files and call NASTRAN solution sequences for the analyses described in the previous sections.

Simply put, one iteration of NASTRAN Sol 106 is used to obtain the deformed wing shape. This shape is used to update the effective angle of attack at various span-wise stations for the next iteration of Sol 144. The converged deformations and mode shapes are imported into Sol 145 where Equation (3.27) is solved for the exact flow conditions as Sol 144. Ferguson et al. [44] implement a similar iterative approach using Visual Basic for nonlinear aeroelastic analysis. This process is summarized in Figure 3.2.

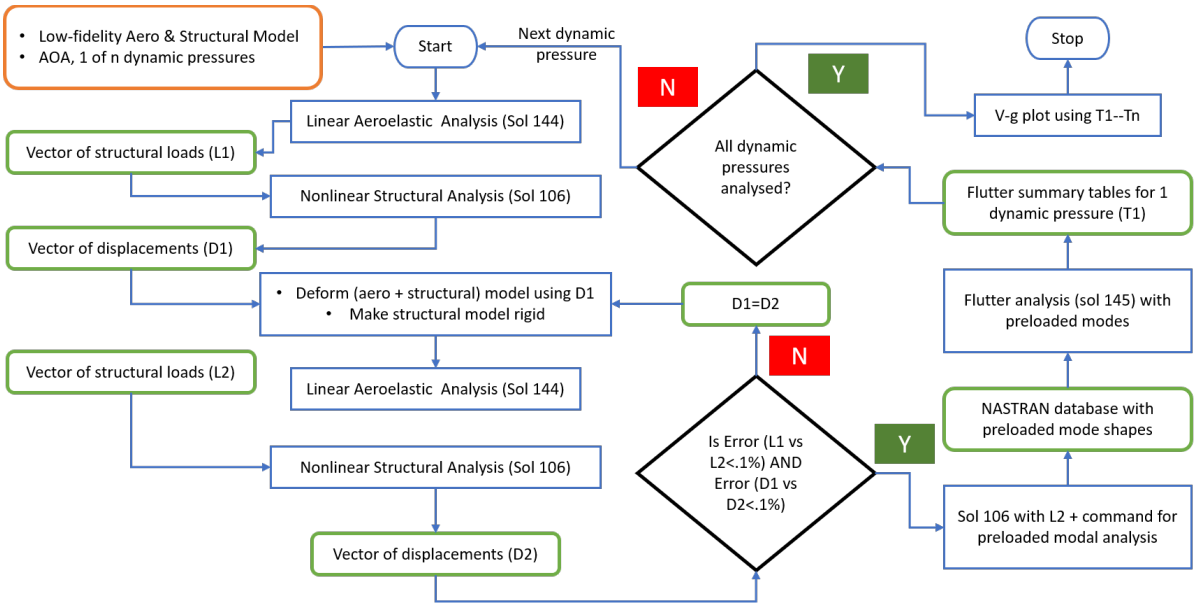

Figure 3.2: Nonlinear iterative aeroelastic analysis

1. **Nonlinear static aeroelastic analysis**

   (a) **Structural model** A bdf file describing the structure of the wing is created. Grid points

(nodes) which will be connected by the beam elements are defined on the global Y axis at 1 m intervals from 0 to $16m$. For each 'beam' node, additional points for lumped masses are created at $X = \pm 0.5m$. The IDs for nodes are designed so that a table of nodal displacements would list the beam node displacements, followed by the displacements of the points at $X = -0.5m$ (the wing leading edge) and finally the displacements of the points at $X = +0.5m$ (the trailing edge). Beam elements connecting the beam nodes are defined. Cross-sectional dimensions and the material properties are specified. Lumped masses of $14.784kg$ each are placed at the 'mass' nodes. Mass and beam nodes are connected using rigid elements. The DOFs of the mass points are made dependent on the beam node DOFs.

(b) **Linear aeroelastic analysis with a flexible structure**: The input file for linear static aeroelastic analysis (NASTRAN solution sequence: Sol 144) is created. Requests for loads and displacements at all grid points and the lift distribution over the wing are made in the case control section. In the bulk data section, the structural file created above is imported and the wing root is clamped. A $16m \times 1m$ lifting panel which uses DLM aerodynamics is created in the XY plane with 32 span wise and 8 chord wise elements. A spline to transfer aerodynamic loads onto the structure is defined. It transfers the loads from all the aerodynamic elements onto the beam and mass nodes. Static aeroelastic analysis parameters are specified. These include the Mach number (which is set to zero to specify incompressible aerodynamics), the dynamic pressure in Pascals, the angle of attack in radians and the vertical load factor in Gs. The file is run and the forces, moments on the beam and mass nodes listed in the output are copied onto MATLAB matrices. Another matrix saves the nodal displacements.

(c) **Nonlinear static analysis**: The input file for nonlinear static analysis (NASTRAN solution sequence: Sol 106) is created. The case control section requests displacements, forces at all grid points and stresses in all beam elements. A sub-case for nonlinear static analysis is defined, with a load set, a constraint set and a set for nonlinear analysis parameters. A request for modal analysis on the converged solution is made. In the bulk data section, the same structural model as Sol 144 is imported. Loads from Sol 144 output are entered as 'follower' loads. The parameters for nonlinear analysis are specified these include the number of increments the load is to be divided into, the number of iterations permitted per increment and the number of iterations after which the stiffness matrix is to be updated. For nonlinear modal analysis, the stiffness matrix has to be updated each iteration and the results have to be saved. So, the nonlinear analysis uses a full Newton-Raphson method. After the parameters for modal analysis are specified, the file is submitted for analysis. A request to save the analysis database is also made. Once Sol 106 converges, NASTRAN saves the output in both the database and the plain text format. The displacements and loads in the text output file are saved as MATLAB matrices.

(d) **Sol 144 with a rigid structure**: Displacements from Sol 106 are added to nodal coordinates from the structural file to get a new set of deformed coordinates. These coordinates are used to create a new structural file with the same element and node IDs as the previous file. The stiffness of the beam elements is increased until the structure is practically rigid. A new Sol 144 input file is also created. Here, the single $16m \times 1m$ panel is replaced by four $4m \times 1m$ panels. The coordinates for the corners of these panels are determined using the Sol 106 displacements of the 'mass' node points connected to every fifth beam node. The rotations at beam nodes from Sol 106 output are used to define the initial incidence of aerodynamic elements in these panels. In this manner, the nonlinear structural displacements and follower force effects are interpolated onto the aerodynamic model. This modified Sol 144 file is submitted for analysis and the loads on structural nodes are extracted and used to create a second Sol 106 file. The analysis parameters, output requests and constraints remain the

same as before.

(e) **Convergence check**: After the second Sol 106 analysis is completed, the displacements are compared with those from the last Sol 106 run. Also, the bending moment at the wing root in Sol 144 (listed as the trimmed OLOAD resultant, component T3, in the Sol 144 output file) from the previous run is compared to the one from this run. Steps 1(b) to 1(d) are repeated until the nonlinear displacements and the aeroelastic reaction load (root bending moment) converge.

2. **Flutter analysis with nonlinear modes**:

   (a) After the static aeroelastic analysis has converged, the saved database from the last Sol 106 solution is imported in the input file for linear flutter analysis (Sol 145). This database includes the nonlinear stiffness matrix and normal modes.

   (b) These modes are imported into the linear flutter analysis module (Sol 145) and the PK flutter method is run for the same dynamic pressure as Sol 144. Normally the flutter solution is run for a range of velocities. However, the aim is to carry out an eigenvalue analysis about the nonlinear static aeroelastic equilibrium condition. Since the modes imported into Sol 145 represent the loads for just one velocity, the flutter solution is asked to calculate complex eigenvalues for just that velocity.

   (c) This process is repeated for all speeds at one AOA and air density. The complex eigenvalues from all the Sol 145 runs are then used to create a velocity vs. damping plot to find the flutter point.

3. Either the angle of attack or the altitude is changed and steps 1 and 2 are repeated. This continues until all the flight conditions have been analysed.

4

Validation

The surest way to verify the results of an analysis is to through experiments conducted under the same conditions as the analysis. If such an exercise is not possible, results from literature can be used in lieu of experimental data. Another alternative is to analyse the same model subject to the same loads, constraints and boundary conditions but using an established/proven method and compare the results. In this thesis, validation was attempted via the last option. This chapter describes the process and the results thereof.

4.1. Validation Using Proteus

Proteus is a Matlab based, nonlinear aeroelastic optimization tool developed by Werter and De Breuker [122]. It models a wing box using nonlinear, Timoshenko beams and couples it to an unsteady vortex lattice method (UVLM) panel code [122]. The 1-D beam representation and the fidelity of the aerodynamic model are similar to those used in NASTRAN. Proteus has been verified experimentally [123]. So, the results of aeroelastic analysis from Proteus can be used to validate the nonlinear iterative method used in this thesis. Proteus can also be used to carry out standard linear aeroelastic and structural analysis. These capabilities offer a way to validate this thesis's analysis method in a detailed, step-by-step manner. The aim is to model the same wing box in Proteus, analyse it under similar loading and boundary conditions and see if similar structural, static aeroelastic and dynamic aeroelastic responses are obtained.

4.1.1. Modelling

A simple, rectangular, untapered and unswept wing box with a 16m half span and a constant 1m chord was modelled in NASTRAN and Proteus. Its hollow rectangular cross-section is $0.85m$ wide and $0.2m$ high with $7.5mm$ thick side walls and $5mm$ thick top and bottom walls. Its elastic axis and centre of mass are coincident and located at mid-chord. The material is assumed to be an aluminium alloy with tensile modulus $E = 72 \times 10^9 Pa$, shear modulus $G = 26.9 \times 10^9 Pa$ and mass density $\rho = 2767.99 kg/m^3$. The wing box is modelled using $1m$ long CBEAM elements in NASTRAN and the number of beam elements is entered as 16 in the Proteus input file. A convergence check using a single static tip load shows the

tip displacement and the total bending moment at the root do not change after the number of beam elements crosses 12 in both NASTRAN and Proteus. However, using 16 elements keeps the element coordinates as nice, round numbers. Mass is simulated by setting $\rho \approx 10^{-9} kg/m^3$ and adding lumped masses ($14.784kg$ each) at 0 and 100% of chord for each structural node. The wing is clamped at the root (i.e. cantilevered). In both NASTRAN and Proteus, the global x-axis is parallel to the direction of the air flow and the global y-axis lies along the wingspan.

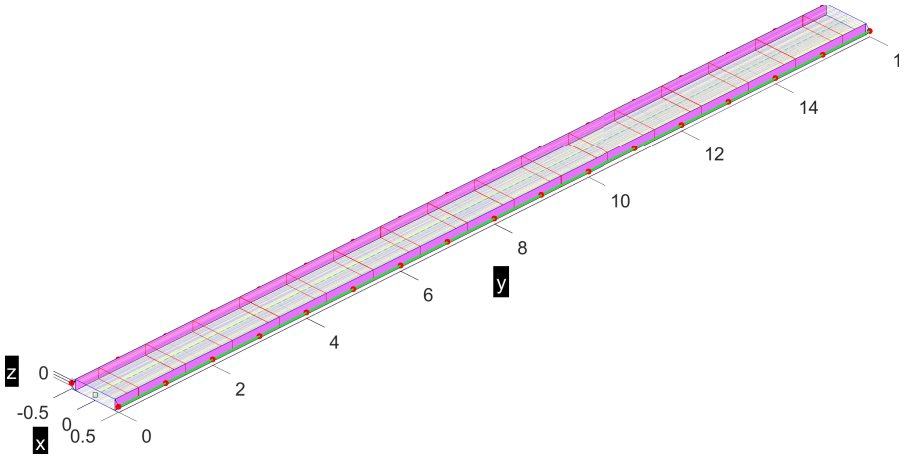

Figure 4.1: Geometry of the wing box, as modelled in Proteus

4.1.2. Structural Response

Proteus and NASTRAN output was compared for the following cases: a single vertical load of 36kN at the wing tip, a single twisting moment (i.e. about the y-axis) of 40kN.m at the wing tip, combined bending and twisting loads ($N_z = 18$kN, $M_y = 5$kN.m, $M_x = 18$kN.m) and linear modal analysis. A very low airspeed ($\approx .001m/s$) was entered in Proteus and the loads were added as 'external forces'. NASTRAN's linear static (Sol 101) and nonlinear static (Sol 106) modules were used. *All forces and moments in the nonlinear static analysis were of the follower type*. The results are presented on the following pages.

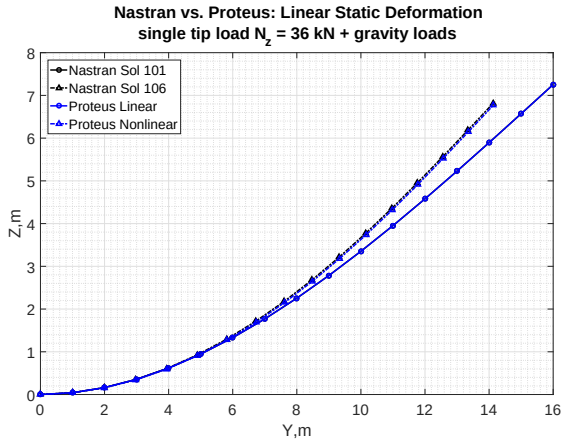

Figure 4.2: Bending displacements

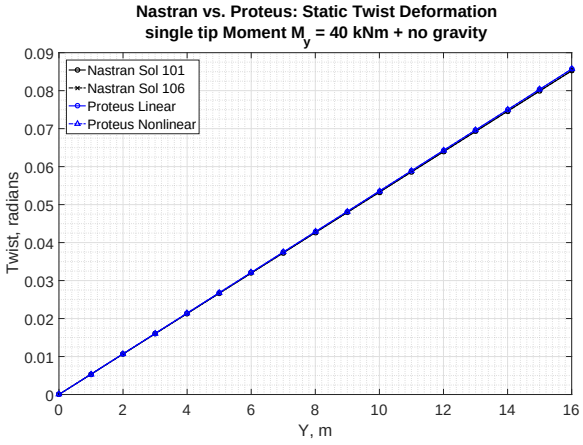

Figure 4.3: Twist angles

For a single tip load and moment, Proteus and NASTRAN give practically identical results (Figures 4.2, 4.3 and Table 4.1). Error in Proteus results w.r.t NASTRAN results is -0.03% (linear, z displacement), -0.57% (nonlinear z displacement) and -0.81% (nonlinear y displacement). For the single twisting moment, the error in twist for all nodes is 0.53% for both linear and nonlinear static analysis

	Bending load ($N_z = 36kN$)				**Twisting moment ($M_y = 40kNm$)**	
	Linear (m)		Nonlinear (m)		Linear (rad)	Nonlinear (rad)
Proteus	$Y \approx 0$	$Z = 7.2524$	$Y = -1.8638$	$Z = 6.7729$	0.0852	0.0852
Nastran	$Y \approx 0$	$Z = 7.2546$	$Y = -1.8790$	$Z = 6.8118$	0.0857	0.0857

Table 4.1: Deformation for single loads: NASTRAN vs Proteus

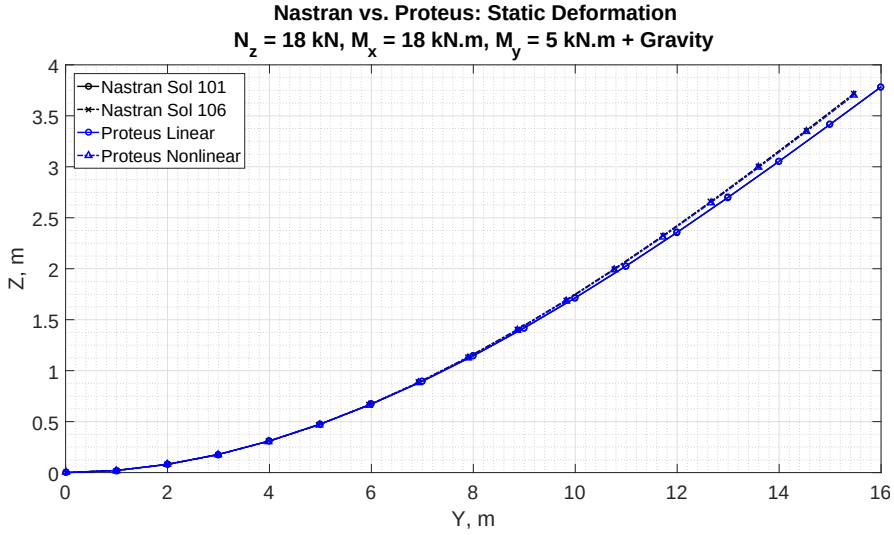

Figure 4.4: Wing deformation due to combined bending and twist tip loads

(Figure 4.3). This shows a good agreement between NASTRAN and Proteus structural models.

To further ensure similitude in the structural response, a bending force, a bending moment and a twisting moment were applied together at the tip of the wing box. Figure 4.4 shows the linear bending deformations to be identical in Proteus and NASTRAN. The nonlinear bending deformations differ by -0.51% and -0.9% in z and y respectively. The bending angle (θ_x), seen in Figure 4.5's left half, also shows good agreement. The error is about -1% for nodes near the root and -0.35% for nodes near the tip, for both linear and nonlinear cases. However, the error for the nonlinear twisting angle (θ_y) is quite high, varying from -94% at the root, to -24.4% at the tip. When the bending force of 18kN was halved, the difference in the nonlinear torsional twist between NASTRAN and Proteus disappeared.

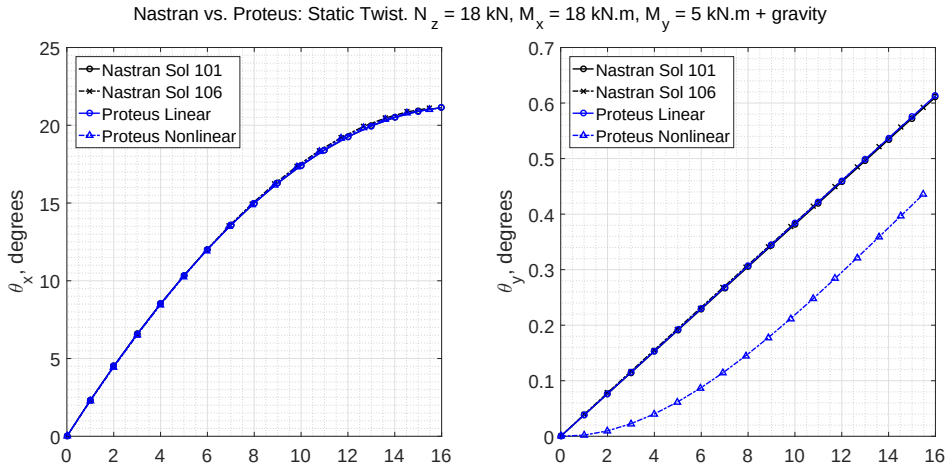

Figure 4.5: Twist at structural nodes due to combined bending and twist tip loads

As seen in Table 4.2, the first five natural frequencies calculated by the two programs are almost

	Rad/s					Hz				
Proteus	6.02	20.243	37.378	95.659	102.961	0.9581	3.22	5.95	15.225	16.387
NASTRAN	6.019	20.244	37.378	95.911	102.979	0.9878	3.22	5.95	15.265	16.389

Table 4.2: First five natural frequencies: NASTRAN vs Proteus

identical. So, the models in the two programs have similar mass distribution and dynamic characteristics. The reason for the difference in θ_y for the combined load case was initially thought to be the way in which combined bending-torsion loads are interpreted by Proteus and NASTRAN. However, the root cause turned out to be the follower force effect. When the direction of forces and moments in the combined load case was fixed in the global coordinate system, the difference in θ_y was negligible. If the follower force effect is turned on and combined bend-twist displacements are involved, the two programs reorient the load vectors differently. This is also reflected in the results of preloaded modal analysis from Proteus and NASTRAN.

Unloaded			**10 kN z**			**10 kNm y**			**10 kN z + 10 kNm y**		
Proteus	NASTRAN	Error (%)	Proteus	NASTRAN	Error (%)	Proteus	NASTRAN	Error (%)	Proteus	NASTRAN	Error (%)
6.020	6.019	0.013	6.034	6.098	-1.060	6.020	6.019	0.014	6.034	6.098	-1.060
20.243	20.244	-0.005	19.711	19.832	-0.610	20.242	20.243	-0.005	19.710	19.831	-0.609
37.378	37.378	0.000	37.155	37.277	-0.327	37.381	37.381	0.000	37.157	37.279	-0.327
95.658	95.911	-0.264	94.950	95.415	-0.487	95.658	95.911	-0.264	94.947	95.411	-0.486
102.960	102.980	-0.020	102.442	102.546	-0.102	102.945	102.964	-0.018	102.433	102.538	-0.102

Table 4.3: Preloaded natural frequencies (rad/s): NASTRAN vs Proteus, non-follower loads

5 kN z			**10 kN z**		
Proteus	NASTRAN	Error (%)	Proteus	NASTRAN	Error (%)
6.023	6.445	-6.538	6.014	7.540	-20.243
20.105	20.064	0.204	20.222	19.546	3.461
37.322	37.402	-0.214	37.342	37.467	-0.332
95.474	95.697	-0.234	95.808	95.098	0.746
102.828	102.853	-0.024	102.869	102.479	0.381

Table 4.4: Preloaded natural frequencies (rad/s): NASTRAN vs Proteus, follower loads

A look at Tables 4.3 and 4.4 leads to a few important observations. Firstly, twisting moments do not have as large an effect on the natural frequencies as bending forces and moments. In Table 4.3 the unloaded natural frequencies are very close to the pre-stressed natural frequencies for the 10 kNm load case. Second, including follower effects in NASTRAN and Proteus creates a difference in the pre-stressed natural frequencies and twist deformations. See Table 4.4, a small vertical load (follower) of 5 kN creates a difference of 6.54% in the first modal frequency. When the load is increased to 10 kN, the first modal frequencies in NASTRAN and Proteus differ by 20%. The difference in frequencies is much less for higher frequency modes. From this, it can also be inferred that results from Proteus and NASTRAN will begin to diverge as the contribution from follower effects increases.

4.1.3. Aerodynamic Response

For aerodynamic modelling, NASTRAN uses the Doublet Lattice Method (DLM) [95] and Proteus uses the unsteady Vortex Lattice Method (UVLM) [122]. Both DLM and UVLM are panel codes based on linear potential flow theory [3, 122]. But whereas DLM is a frequency domain solver [3], UVLM works in the time domain [122]. To check the equivalence of aerodynamic models, wings in both software were modelled as a single lifting surface (panel). The same number of aerodynamic elements (boxes) in the span and chord wise direction was specified. The structural model was made very stiff, practically rigid, and the same flow conditions were analysed in NASTRAN and Proteus.

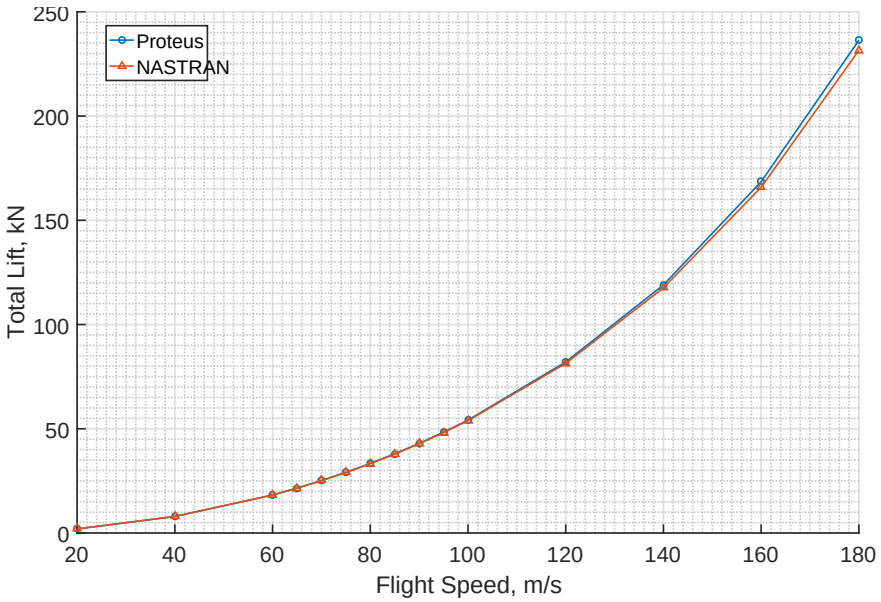

Figure 4.6: Total lift for a rigid wing: NASTRAN vs Proteus, $5°$ AOA, sea level

The total lift in NASTRAN and Proteus shows good agreement (Figure 4.6). The difference is about $-.1\%$ at $20m/s$ and 2.1% at $180m/s$. The span-wise lift distribution was different initially. Proteus automatically makes the panel mesh finer at the tip and the root. In NASTRAN, unless otherwise specified, all panel boxes are of equal width. With identical panel box widths, the difference in lift distribution was less than 2% at any span-wise station (Figure 4.7). The lift coefficient (C_{l_α}) in NASTRAN was 5.89 versus 5.9 in Proteus. These results show a good match in the aerodynamic response.

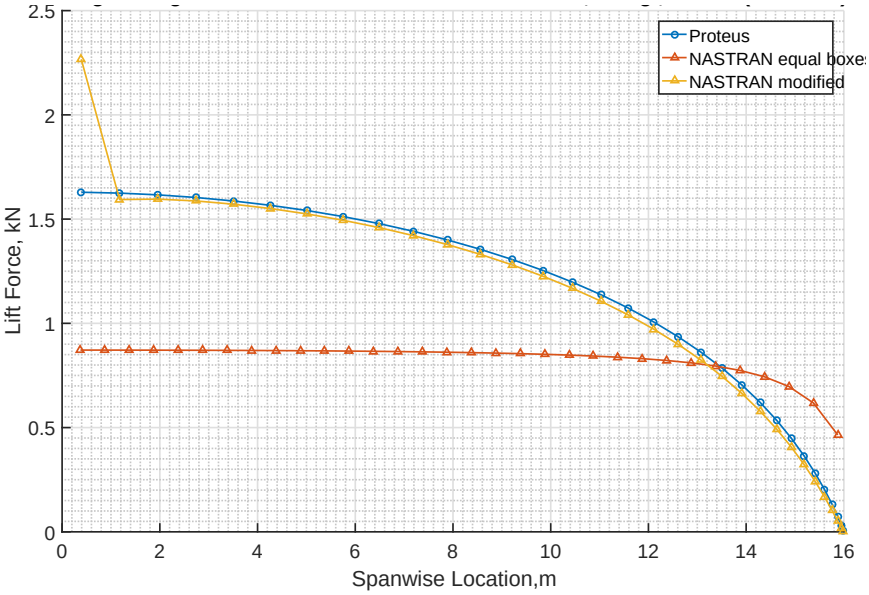

Figure 4.7: Lift distribution across wingspan for a rigid wing: NASTRAN vs Proteus, $80m/s$, $5°$ AOA, sea level

4.1.4. Static Aeroelastic Response

Linear and nonlinear static aeroelastic analyses were carried out for a fixed flow speed of 80 m/s at sea level (dynamic pressure $q = 3920Pa$) and AOA $= 2.5° - 10°$. The linear static aeroelastic deformations match reasonably well for Proteus and NASTRAN, as seen in Figure 4.8 and Table 4.5.

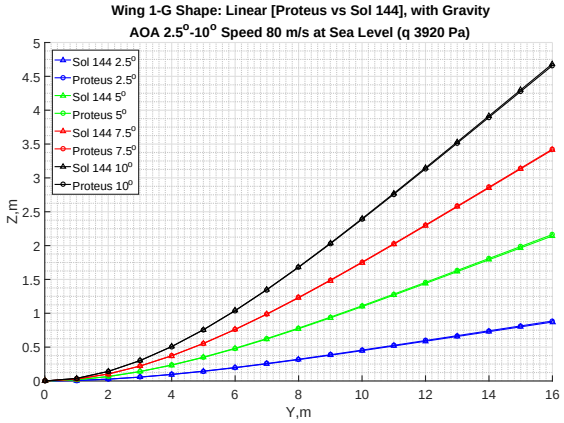

Figure 4.8: Linear aeroelastic deformations

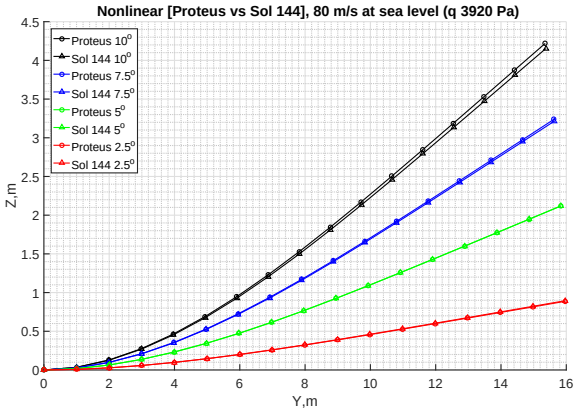

Figure 4.9: Nonlinear aeroelastic deformations

	Linear aeroelastic				Nonlinear aeroelastic			
AOA (°):	2.5	5	7.5	10	2.5	5	7.5	10
Tip Disp. (z) Error (%)	1.7186	1.007	0.3133	-0.55875	-0.942	-0.082	0.799	1.596
Tip Disp. (y) Error (%)	N/A				0.0034	0.0022	-0.036	-0.128

Table 4.5: Error in static aeroelastic results: NASTRAN vs Proteus

The difference in aeroelastic displacements between Proteus and NASTRAN is within acceptable limits. But it shows a trend of changing from negative to positive (nonlinear Z displacement, Table4.5) and vice versa (linear case) as the AOA is increased from $2.5°$ to $10°$. Most likely, this is because of a difference in the aerodynamic loads calculated by DLM and UVLM. To make sure there are no major differences between the NASTRAN and Proteus models, the nonlinear analysis was rerun at $100m/s$ for the 4 AOA values. Results are shown in Figure 4.10.

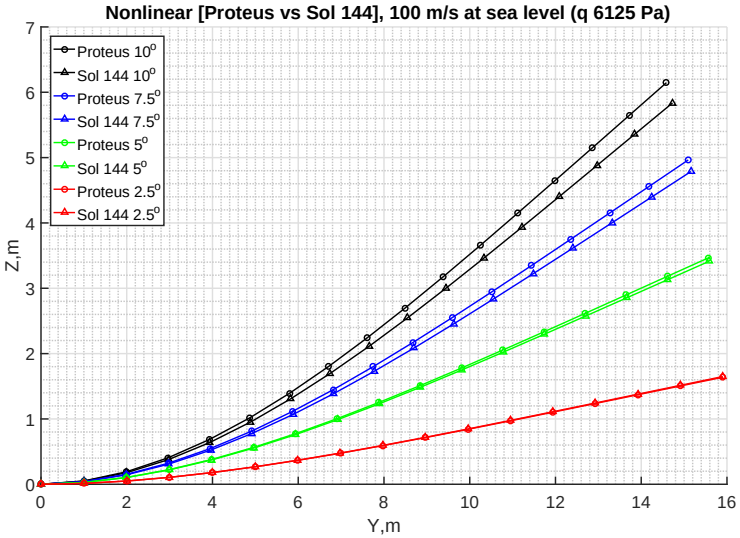

Figure 4.10: Nonlinear aeroelastic deformations: NASTRAN vs Proteus, $100m/s$

The error is still acceptable ($< 4\%$) for AOA up to $7.5°$, but it is almost 6% for $10°$. This should not be taken to mean that the analysis results are not reliable. The tip vertical deflection for an AOA of $10°$ at $100m/s$ is $\approx 6.1m$, almost 40% of the wing half-span. The results for such high deflections have to be taken with a grain of salt. It is reasonable to conclude that the nonlinear iterative method is reasonably accurate as long as the wing tip deflection is less than 30% of the half-span.

AOA (°)	2.5	5	7.5	10
Tip Disp. (z) Error (%)	-0.6	1.754	3.96	5.58
Tip Disp. (y) Error (%)	.008	-1.02	-.484	-1.08

Table 4.6: Error in nonlinear static aeroelastic results at $100m/s$

4.1.5. Flutter Analysis

As stated earlier (Chap. 4), geometric nonlinearities are included in the flutter analysis by using pre-stressed normal modes calculated at the nonlinear static aeroelastic equilibrium condition. These modes are imported in NASTRAN's flutter analysis module, Sol 145 and the PK method is used to generate 'flutter summary tables' at each velocity. These tables are collated to generate the flutter diagrams. The nonlinear flutter analysis results were verified in two ways.

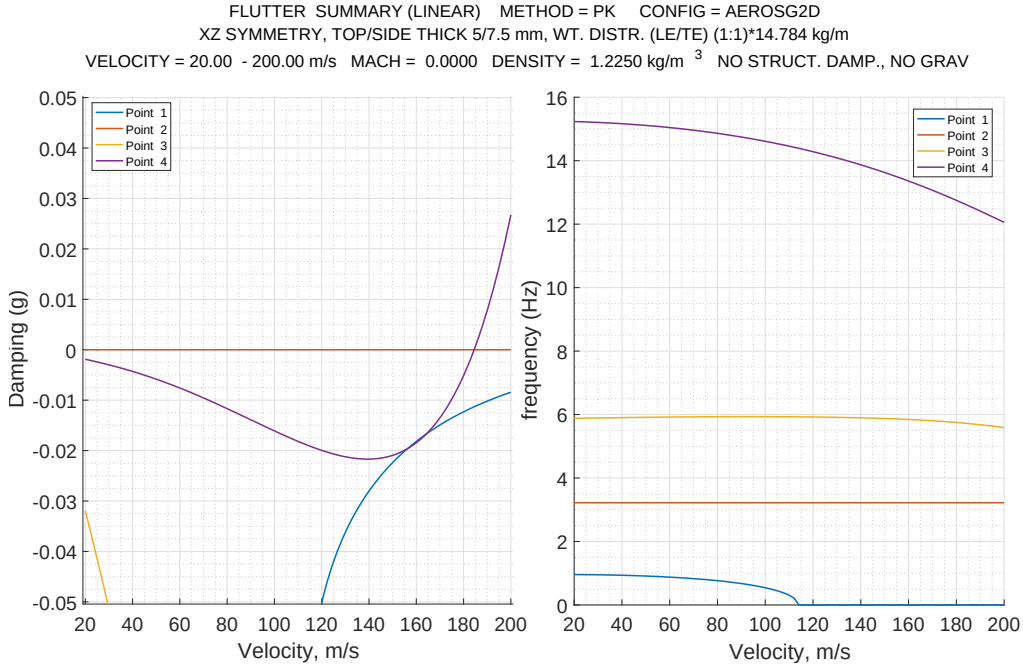

Figure 4.11: Linear flutter plot: NASTRAN Sol 145

First, the nonlinear flutter solution was run for an angle of attack close to zero. It was expected that the results would match, or get very close to, standard Sol 145 analysis results (Figure 4.11) as the AOA approached zero. A look at Table 4.7 and Figure 4.12 shows that this is indeed the case. The nonlinear flutter speed (V_f) was 2.37% higher than the linear V_f. The frequency of the critical mode at V_f (the flutter frequency, ν_f) is 1.27% lower. Qualitatively, the behaviour of the modes (change in damping and frequency with speed etc.) was identical to the linear case. In both cases the critical mode is mode

	Linear Sol 145 (base)	Nonlinear (AOA $.0001°$)	Error (%)
Flutter speed	$184.4m/s$	$188.8m/s$	2.37%
Flutter frequency	$12.6Hz$	$12.44Hz$	-1.27%

Table 4.7: Linear vs nonlinear flutter results: NASTRAN

4. It has a coupled, bending-torsion mode shape. The frequency of mode 1, first bending, drops to zero at around $115m/s$. Had the damping of this mode crossed zero, it would have indicated divergence [95]. But the mode remains damped. However, its $V-g$ curve becomes discontinuous at the same speed at which its frequency drops to zero. Mode 2 is the in-plane or edgewise bending mode. Since DLM does not consider drag effects, the damping of this mode is always very close to zero. Thus, the

instabilities involving this mode cannot be taken at face value. It goes without saying that Figures 4.11 and 4.12 do not show all the modes over all the velocities for the sake of clarity. Modes with very high frequencies and/or very negative damping values are not shown.

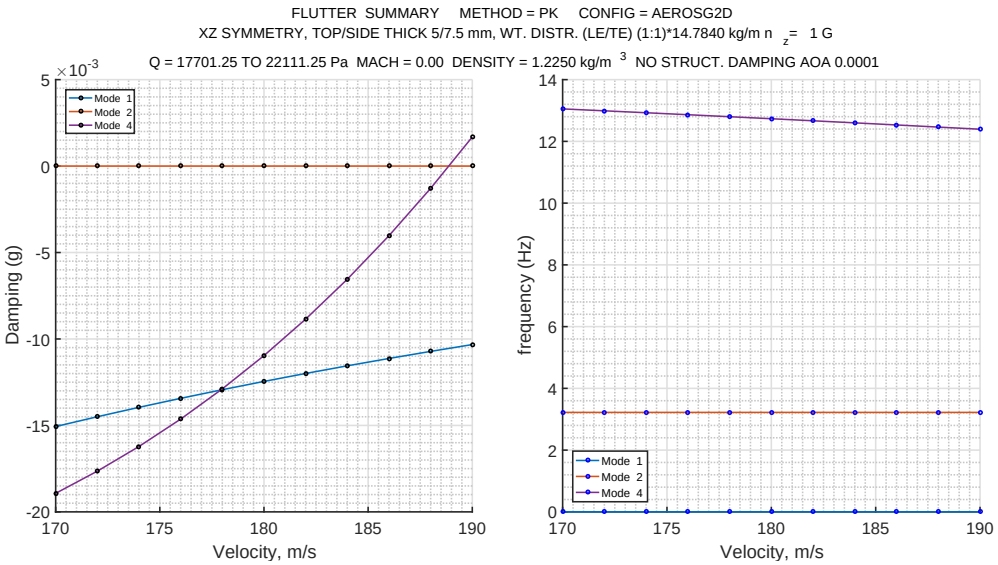

Figure 4.12: Nonlinear-iterative flutter plot for AOA .001°

Next, Proteus was run in linear mode with AOA $= 0°$ and in nonlinear mode with AOA $= 0.0001°$. In both cases, velocities distributed about the linear V_f from Table 4.7 were specified in the 'load case' section. Finally, the results for nonlinear flutter analysis at $2°$ in NASTRAN and Proteus were compared.

Proteus calculates complex eigenvalues for each load case by using the structural stiffness and aerodynamic influence coefficient (AIC) matrices and saves them in the dynamic aeroelastic output section. The real and imaginary parts of these eigenvalues can be used to get damping and reduced frequencies akin to those calculated by NASTRAN. If the complex eigenvalue for an aeroelastic mode at a velocity V is (Equation 2-133, [95] and Equation 2.29, [60]):

$$p = \sigma \pm \omega i = \omega(\gamma \pm i) \tag{4.1}$$

The reduced frequency (k) is given by (Equation 2-134, [95]):

$$k = \omega\left(\frac{\bar{c}}{2V}\right) = \left(\frac{\bar{c}}{2V}\right)\text{imag}(p) \tag{4.2}$$

Here, $\bar{c}$ is the reference chord and ω is the mode frequency in rad/s. The damping g is given as (Equation 2-136, [95]):

$$g = 2\gamma = 2\frac{\text{real}(p)}{\omega} \tag{4.3}$$

It should be noted that, if the frequency of a mode drops to zero, as it does for mode 1 in Figure 4.11, damping given by Equation (4.3) would be infinite. NASTRAN may use other formulas to obtain the damping in such cases. To avoid infinite damping, the angular frequency (ω^P) for Proteus' complex eigenvalues is calculated as follows:

$$\omega^P = \sqrt{\text{real}(p)^2 + \text{imag}(p)^2} = \sqrt{\sigma^2 + \omega^2} \tag{4.4}$$

Equation (4.4) and (4.3) can be used to derive damping values, create velocity-damping ($V - g$) plots and find the flutter speed. For these plots to be accurate though, the velocities for successive load

cases in Proteus have to be close to each other. This is because Proteus uses MATLAB's in-built eigenvalue function to calculate the complex eigenvalues. The stability of a mode at a certain speed is proportional to the magnitude of the real part of the corresponding complex eigenvalue (Equation (4.3)). The most 'critical' eigenvalues are listed in decreasing order of their real part. Suppose we specify 10 load cases in Proteus, each load case for an airspeed $5m/s$ higher than the last load case. If we take the damping from the first eigenvalue listed for each load case and plot it, odds are we would not be tracing the same mode from one velocity to the next. The only solution to this seems to be to keep the velocity for one load case within $1m/s$ of that from the previous load case and to cover a wide range of velocities.

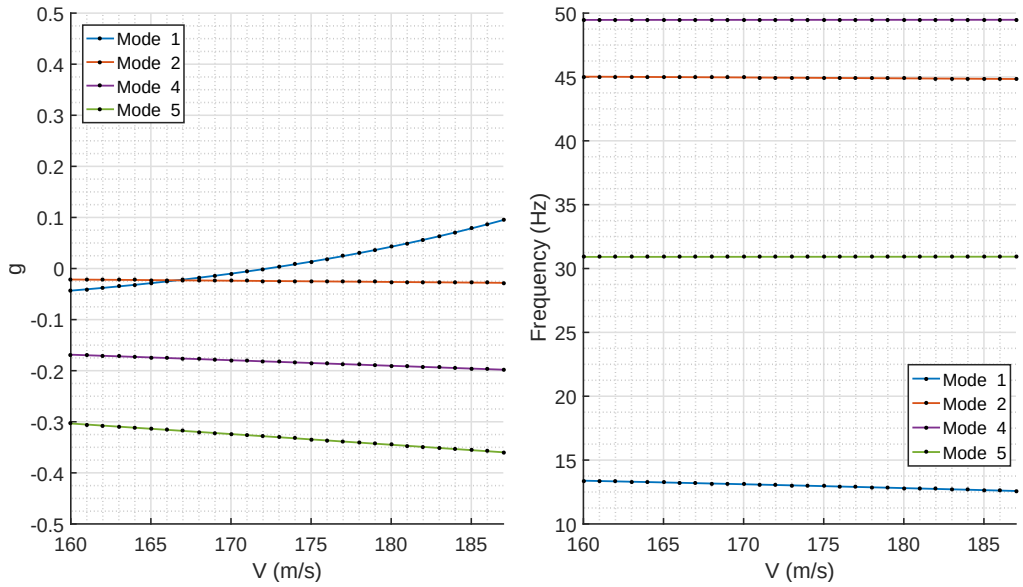

Figure 4.13: Flutter plot: linear Proteus run at 0° AOA, 0 km, 0 Mach, gravity 'off'

For the linear case (Figure 4.13), Proteus gives a flutter speed of approximately $172.3m/s$ and a flutter frequency of $13.04Hz$. With respect to these values, NASTRAN's Sol 145 gives a 7% higher V_f and a 3.4% lower ν_f. For nonlinear flutter analysis at an AOA very close to zero, Proteus nonlinear

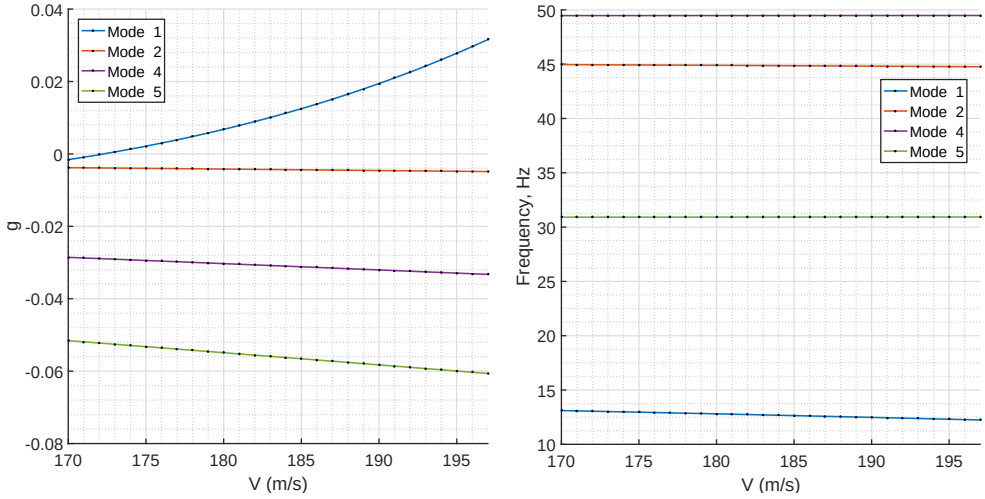

Figure 4.14: Flutter plot: nonlinear Proteus run at 0.0001° AOA, 0 km, 0 Mach, gravity 'off'

results are identical to its linear results (Figure 4.14). As seen from Table 4.7, NASTRAN linear and nonlinear results differ by 2.4% for V_f and 1.3% for ν_f. These errors are small, but the exact match between Proteus linear and nonlinear results is quite surprising.

At $2°$ AOA, flutter occurs at $203m/s$ and $13.39Hz$ according to Proteus (Figure 4.15). NASTRAN nonlinear flutter analysis shows a higher V_f of $233m/s$. The flutter frequency is closer to Proteus at $13.67Hz$. At these speeds, the wing tip vertical displacement is about $8m$, i.e. half of the wing half-span. At such large displacements, the the differences in follower force effects and aerodynamic response in the two programs have a greater on the final result. Since the flutter frequencies match up reasonably well, we can assume that the structural responses predicted by NASTRAN and Proteus are close to each other. The results for all three cases are summarised in Table 4.8.

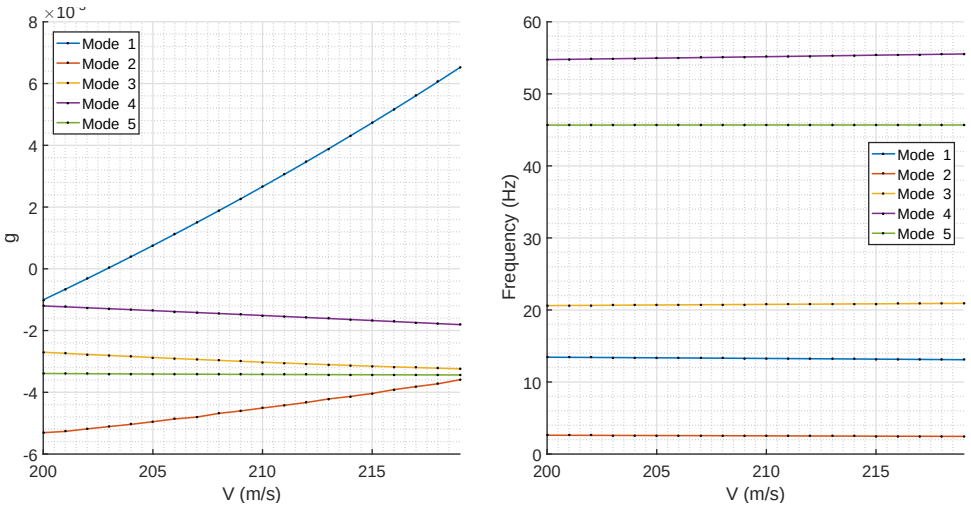

Figure 4.15: Flutter plot: nonlinear Proteus run at $2°$ AOA, 0 km, 0 Mach, gravity 'off'

	Linear			Nonlinear $0.0001°$			Nonlinear $2°$		
	NASTRAN	Proteus	Error (%)	NASTRAN	Proteus	Error (%)	NASTRAN	Proteus	Error (%)
V_f (m/s)	184.40	172.30	7.02	188.80	172.30	9.58	233.0	203.0	14.78
ν_f (Hz)	12.60	13.04	-3.37	12.44	13.04	-4.60	13.67	13.39	2.09

Table 4.8: Proteus vs NASTRAN flutter results

It should also be noted that all the flutter calculations use generalised coordinates. The approach to generalising displacements, stiffness coefficients etc. might differ in NASTRAN and Proteus and this would certainly have an effect on the results. One way to account for these differences would be to relax the $0g$ criterion. That is, instead of noting the exact speed at which a mode crosses 0, a mode would be considered unstable when its damping reaches a certain value above zero (of the order of magnitude 10^{-3}). In conclusion, the nonlinear iterative method was validated against Proteus for static structural, static aeroelastic and flutter analyses. The results showed a good agreement for moderate tip vertical deflections ($\approx 30\%$ of the half span).

4.2. Attempted Validation Against Patil's Results

It was initially decided to recreate the HAR wing of the HALE drone model analysed by Patil et al. [86] and compare the results of static aeroelastic and flutter analyses. However, journal articles and conference papers offer a limited amount of space to authors in which to share their findings. Often, certain assumptions, boundary conditions and other parameters used in the analysis are omitted. In the case of PHC, the journal articles in question are based on Patil's PhD thesis [81]. Both the journal articles and the dissertation list the structural properties of wing in terms of its stiffness and mass moment of inertia ("Table 5.4: HALE aircraft model data", Patil [81] and "Table 1 Aircraft model data",

Patil et al. [86]). Cross-section dimensions, material properties like extension and shear modulus are not mentioned. NASTRAN allows modelling a beam in two ways [66]. The cross-sectional shape can be chosen from an in-built library and its dimensions specified (the PBEAML card, [66]). Or, the cross-sectional area and the area moments can be entered directly (the PBEAM card, [66]). In both cases, a material card with the extension and shear moduli and the Poisson's ratio is required. The cross-sectional properties were solicited from the authors in an online forum where the paper [86] was shared by them. Dr Hodges was kind enough to reply. He suggested using the stiffness as input in a custom 'beam code' and stated "I doubt that the results obtained for this problem would depend significantly on extensional stiffness". His timely response was much appreciated. But the extensional stiffness is needed to derive the quantities required to model the HALE wing in NASTRAN.

Several attempts to back-calculate the cross-sectional dimensions and material properties from the data provided by Patil were made. In a last-ditch attempt, the stiffness and mass per unit length provided were divided by the E, G and ρ of the aluminium alloy Al 7075 T6. The area and area moments were entered in the fields of the PBEAM card. The wing box was modelled using 16 CBEAM elements. The wing elastic axis and centre of gravity were assumed to be coincident and located at the semi-chord ($0.5c$). The mass was decoupled from the stiffness by leaving the density field blank on the material property card and using lumped mass elements connected to the beam nodes using rigid bar elements. The magnitude of these point masses and their distance from the beam axis were varied in an attempt to match the structural natural frequencies to the analytical values listed by Patil in his PhD thesis ("Table 5.5: Comparison of linear frequency results (rad/s) for HALE wing", Patil [81]). The final attempt managed to create a model with properties very close to those mentioned in PHC's work. This version had lumped masses of $.340kg$ each placed at $\pm.369c$ for each beam node. The wing box was about $.6kg$ lighter than Patil's. But linear natural frequencies obtained were $\approx \pm 1\%$ of the analytical values listed by Patil [81] (see Table 4.9 below).

Mode Shape	Analytical, Patil [81]	NASTRAN	Error (%)
1st Flat-wise Bending	2.243	2.216708	−1.172%
2nd Flat-wise Bending	14.056	13.92078	−0.962%
3rd Flat-wise Bending	39.356	39.05052	−0.776%
1st Torsion	31.046	31.27474	+0.737%
1st Edge-wise Bending	31.718	31.30597	−1.299%

Table 4.9: Natural frequencies (rad/s) Patil [81] vs. recreation in NASTRAN

Castellani et al. [17] analyse the same HALE wing and, in addition to the data provided by Patil [81], give the tip displacements for the wing box due to single vertical tip loads ("Table 3 Tip vertical displacement and shortening vs force: follower force"[17]). The wing box recreated in NASTRAN compares well in this aspect too (Table 4.10).

Load:	$25N$			$100N$			$200N$		
	"Table 3" [17]	NASTRAN	Error (%)	"Table 3" [17]	NASTRAN	Error (%)	"Table 3" [17]	NASTRAN	Error (%)
Z (m)	1.7	1.7002	0.012	6.409	6.432	.362	10.754	10.914	1.489
Y (m)	−.109	−.1088	−.212	−1.650	−1.656	.374	−5.662	−5.740	1.375

Table 4.10: Deformation for a single follower load at the tip: Castellani et al. [17] vs. recreation in NASTRAN

While the static and dynamic structural responses matched quite well with the results from literature [17, 81, 86], the linear aeroelastic results diverged. As seen in Table 4.11, NASTRAN predicts a 6.9% higher divergence speed and while a $\approx 3\%$ difference in flutter speed might be acceptable, the flutter

frequency differs by $\approx 6\%$. This dissimilarity can be attributed to the difference in structural frequencies, weight and aerodynamic modelling.

	Patil [81]	NASTRAN	Error (%)
Divergence speed (m/s)	37.29	39.87	6.92%
Flutter speed (m/s)	32.21	31.23	−3.04%
Flutter frequency (rad/s)	22.61	24.002	6.16%

Table 4.11: Linear divergence and flutter results: Patil [81] vs recreation in NASTRAN

Further verification using results from Patil et al. [86] was not pursued for two reasons. First, NASTRAN uses the 3-D panel code, DLM [3], whereas PHC [86] use a 2-D, finite state air loads model by Peters and Johnson [88]. In this model, the effects of the tip and out-of-plane vortices are not considered [81]. This creates a difference in the aerodynamic and subsequently, the aeroelastic response between NASTRAN and Patil's analysis.
Second, NASTRAN calculates the generalized aerodynamic force coefficient (GAF) matrices for use in its flutter solution at the Mach (M), reduced frequency (k) pairs provided by the user. Matrices for (M,k) values other than those specified are interpolated. An injudicious choice of (M,k) pairs can lead to incorrect flutter results. To get the results listed in Table 4.11, a very large number of (M,k) pairs had to be used. This increased the computation time for the linear flutter solution to about 8 minutes. Using the same parameters for the nonlinear flutter solution would make the simulation very slow. A way to calculate GAF matrices once and then import them for each new nonlinear flutter analysis run is not known to the author. Hence, the analysis of Patil's HALE wing [81] was not pursued further.

5

Results

In this chapter, the results of nonlinear static aeroelastic and flutter analyses are discussed. The effect of geometric nonlinearities is examined by comparing the results to those of linear analysis. Some of these results have already been presented in Chapter 4. This chapter examines them in more detail.

5.1. Nonlinear Wing Deformation

Figures 5.1 and 5.2 compare the displacement of the wing tip in z and y directions from linear and nonlinear static aeroelastic analyses (SAA). The linear SAA module works on the 'small displacements' assumption and does not consider bending deformation along the y axis. As a result, the linear analysis begins to over predict the wing deformation as the loads acting on the wing increase.

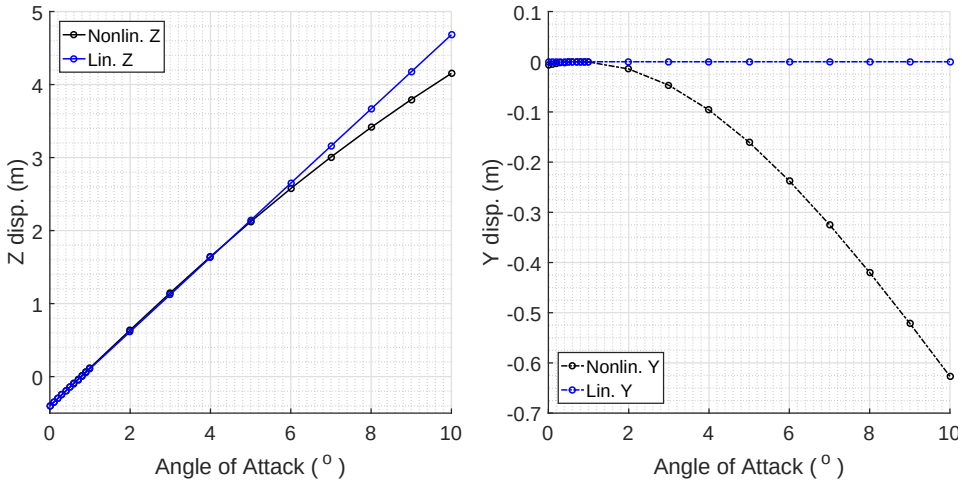

Figure 5.1: Change in linear and nonlinear tip displacements with AOA at 80 m/s airspeed, sea level, gravity 'on'

Simply put, the nonlinear static solver uses a part of the bending load for deformation in the y-direction (tip shortening) and the rest for deformation in the z-direction. The linear solver uses all of the load for deformation in the z-direction. The difference between linear and nonlinear predictions for the z displacement is readily apparent after AOA$= 6^{\circ}$ in Figure 5.1 and somewhat less pronounced in

Figure 5.2. The difference in y displacement is much more visible in both cases. It can also be inferred that the change in loads due to a change in the angle of attack at a fixed speed is more than that due to an increase in speed at a fixed angle of attack.

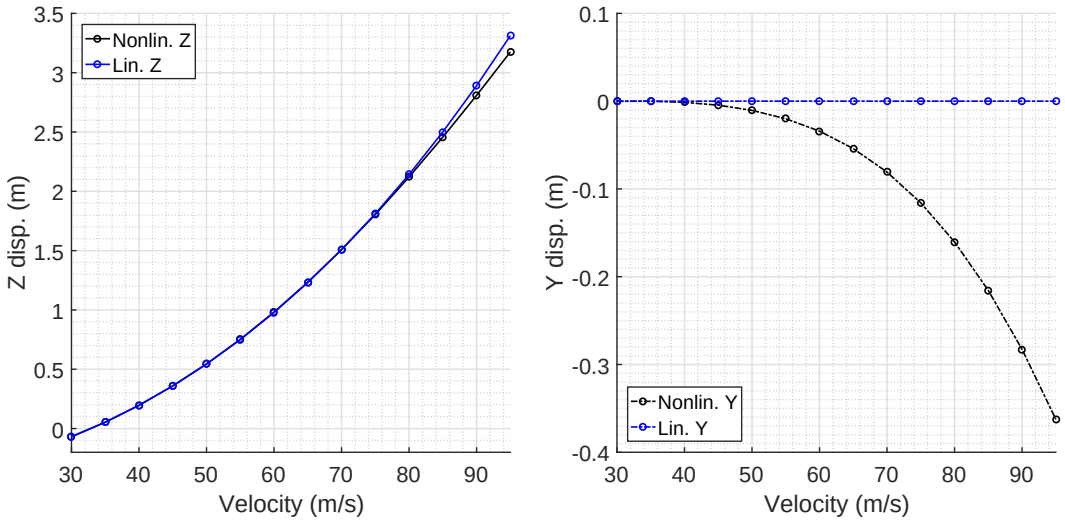

Figure 5.2: Change in linear and nonlinear tip displacements with airspeed at 5° AOA, sea level, gravity 'on'

The effect of including nonlinear deformations in aeroelastic analysis is seen in Figure 5.3. The legend entries 'Sol 144' and 'Sol 106' refer to output from NASTRAN's linear aeroelastic and nonlinear static modules respectively. As indicated by the black arrows, in the first iteration, linear SAA over predicts the vertical displacement, ignoring any displacement along the span. Nonlinear static analysis using the interpolated structural loads from the linear SAA shows deformations in both y and z. The vertical displacement is less but the rotation of each span wise section about the x-axis greater.

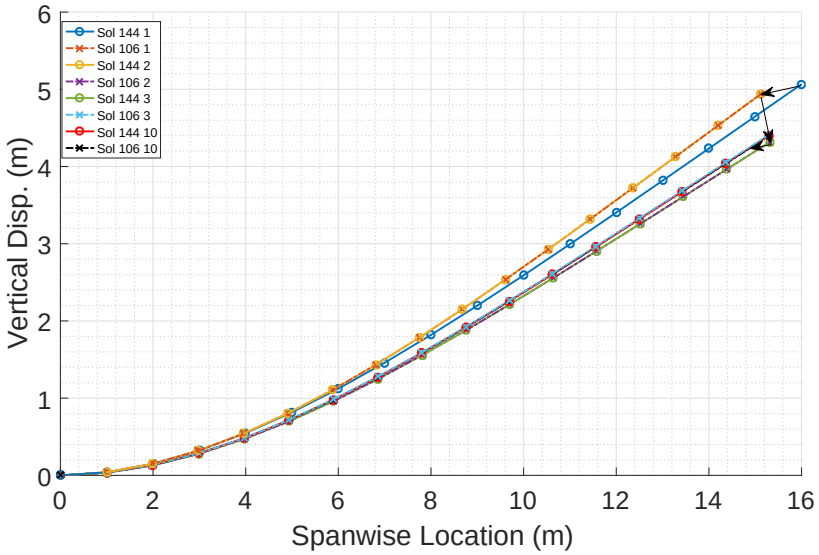

Figure 5.3: Convergence to a nonlinear wing deformed shape

For the second iteration, the nonlinear deformed shape is used to create a rigid wing. This is why, in the figure, Sol 144 displacements from iteration 'n' seem to overlap the Sol 106 results from iteration 'n-1'. Each section of this rigid wing is at a larger angle w.r.t the global Z direction than the wing from the previous iteration. Consequently, the component of lift normal to the lifting panels is smaller; as are the loads interpolated onto the structural nodes. These loads result in smaller z and y displacements

in the next iteration of nonlinear static analysis. This reduces the rotation of span wise sections about the x axis. The rigid wing mimicking this shape gives loads which are higher than the last iteration. In each iteration, the rigid wing shape, the air loads and the nonlinear displacements continue to vary by smaller amounts until converging to the nonlinear equilibrium condition. The deformed shape of the wing in this equilibrium is markedly different from what is predicted by linear SAA.

5.2. Pre-stressed Modes

The nonlinear stiffness matrix for the converged equilibrium condition in Figure 5.3 consists of the linear (or material) stiffness matrix, $[K]^L$, the differential stiffness matrix, $[K]^d$ and the follower force stiffness matrix, $[K]^f$ (Equation (3.3)). $[K]^d$ depends on the deformed geometry of the structure and the applied loads. $[K]^f$ includes the change in orientation of the load vectors as they follow the structural deformation, i.e. the follower effect. Modal analysis using $[K]^T$ in place of $[K]^L$ for nonlinear modal analysis gives the preloaded modes for a structure (Equation (3.6)). This captures the nonlinear effects of applied loads on the natural mode shapes of a structure.

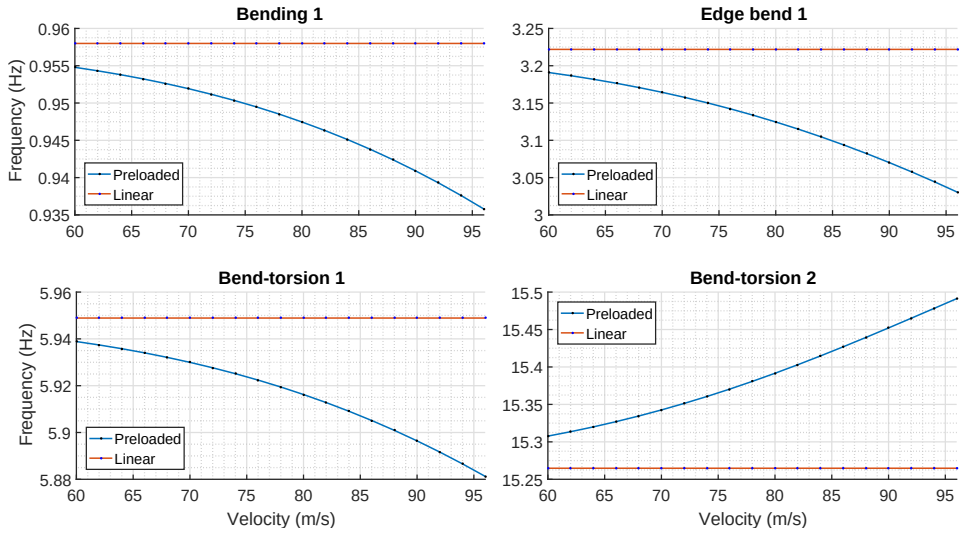

Figure 5.4: Change in the first four natural frequencies with airspeed at 5° AOA, sea level

Figures 5.4 and 5.5 show variation in the first four modal frequencies with increasing loads. The applied loads, in this case, are exclusively aerodynamic loads. The change in their magnitude is proportional to the change in airspeed or the angle of attack, i.e. the flight parameters. Tracking the change in mode frequencies with AOA or airspeed is therefore a reasonable way to monitor the effects of applied loads on these frequencies. As seen in Figure 5.4, the magnitude of the change is relatively minor over a range of $35m/s$. The first bending frequency reduces by about $.015Hz$, the edge bending frequency by $.15Hz$ and the third frequency (the first bend-torsion mode) drops by $.14Hz$. The frequency of mode 4 (second bending-torsion), however, increases by about $.2Hz$. The graphs for all four modes are continuous and consistent. So, it is reasonable to assume that the frequency for the first bending mode would continue to drop with increasing airspeed and that of mode 4 would continue to rise.

Tracking the changes in frequency with the change in AOA (Figure 5.5) shows a trend similar to Figure 5.4. But here we also see the nonlinear/pre-stressed frequencies approach the 'unloaded' linear frequencies as the angle of attack approaches zero. This is because in DLM unless the camber or initial incidence of a wing is specified explicitly, a wing generates zero lift at zero AOA [95]. Also worth mentioning, the 'preload' in these modes is due to the bending-twist air loads acting on the wing. As a

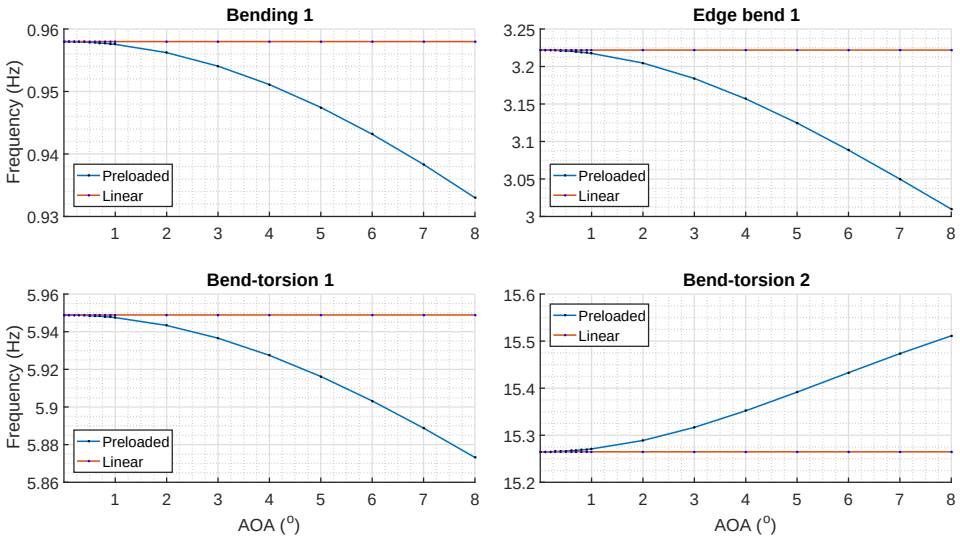

Figure 5.5: Change in the first four natural frequencies with AOA at $80m/s$, sea level

result, modes 2 to 4 change from pure bending or torsion to coupled bend-torsion shapes. However, mode 1 continues to be a pure bending mode. This behaviour may be tied to the frequency of the first aeroelastic mode dropping to zero and its $V-g$ curve being discontinuous (Figure 4.11). Therefore, it might merit further investigation.

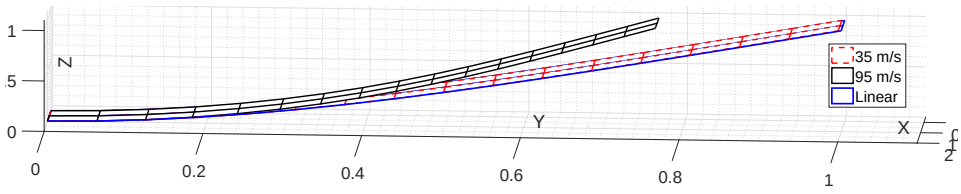

Figure 5.6: Change in normalised shape of mode 1 with airspeed at $5°$ AOA, sea level

The normalized modes shapes for mode 1 (first bending) and 4 (second bend-torsion) at two different airspeeds are shown in Figures 5.6 and 5.7. Both mode shapes change noticeably for a change in airspeed of $60m/s$. These figures, taken together with Figures 5.4 and 5.5 show that even a small change in the modal frequency can indicate a significant change in the mode shape. In the p-k flutter method, the structural mode shapes are used for calculating the initial estimated displacements in generalised (i.e. modal) coordinates ("Chapter 2, The PK-Methods of Flutter Solution", [95]). If these modes include geometric nonlinear effects and preload (via the use of $[K]^T$ in the eigenvalue problem, Equation 3.6), these effects would be included in the flutter solution as well.

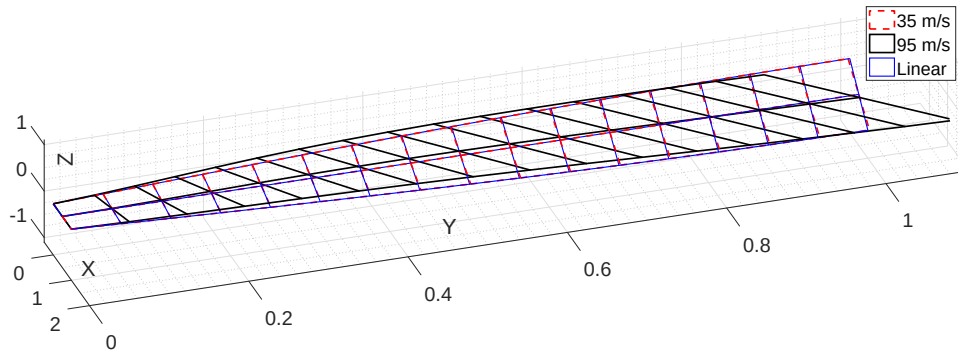

Figure 5.7: Change in normalised shape of mode 4 with airspeed at $5°$ AOA, sea level

5.3. Nonlinear Flutter Analysis

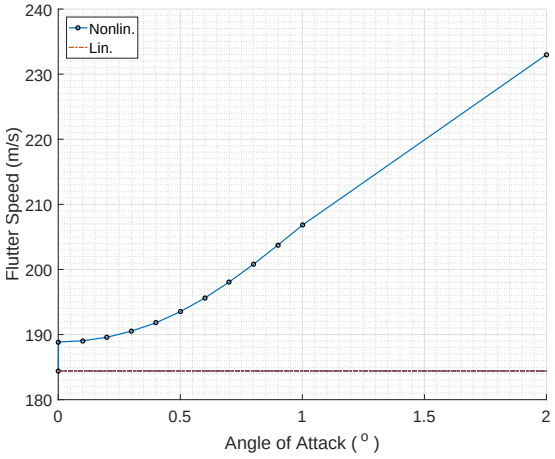

Figure 5.8: Flutter speed vs AOA at sea level

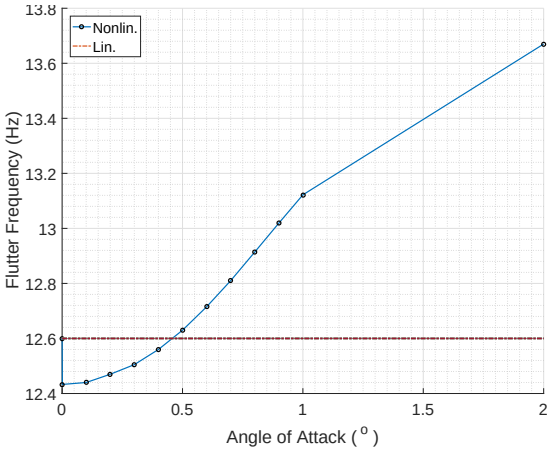

Figure 5.9: Flutter frequency vs AOA at sea level

The nonlinear flutter analysis described in earlier chapters was run for a fixed altitude (sea level) and a range of speeds and AOAs. It is essentially the standard, linear p-k flutter analysis but with nonlinear mode shapes included at each velocity. The results are shown in Figures 5.8 and 5.9. The linear flutter module, Sol 145, gives the same flutter speed and frequency even if the AOA is changed by specifying an initial angle of incidence for wing. The nonlinear results show the flutter speed and frequency rising consistently with the angle of attack.

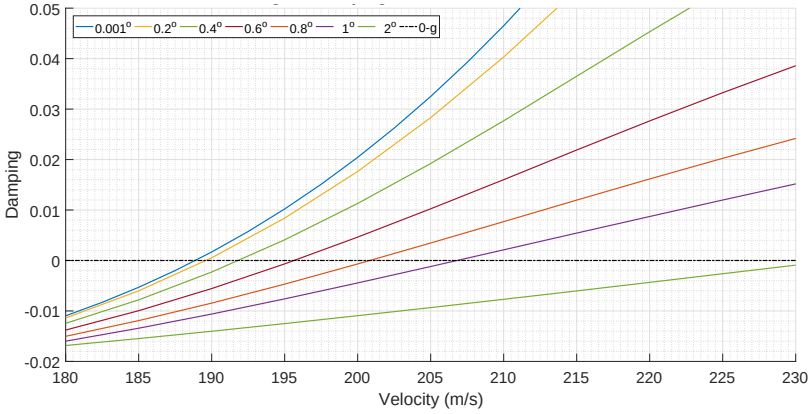

Figure 5.10: Change in damping shape of critical flutter mode with AOA

The reason behind this is the increase in the natural frequency of the critical mode, mode 4, with increasing air loads (Figures 5.5 and 5.4). The higher frequency of this mode translates into higher damping, as seen in Figure 5.10. The speed at which this mode crosses the zero-damping axis and becomes unstable, increases from $188.8m/s$ at $.001°$ to $\approx 233m/s$ at $2°$.

The graphs in Figures 5.8 and 5.9 stop at $2°$ AOA because the wing deformation becomes too high for AOA $> 2°$ and speeds $> 235m/s$. The wing bending deformation is so high that the nonlinear static solution does not converge. At such excessive deformation, flutter becomes a moot point. This peculiar behaviour, where flutter does not occur even when the wing is almost bent into a tube, is a side-effect of the arbitrary structural properties of the wing box. Nevertheless, the nonlinear method successfully demonstrates the effect geometric nonlinearities have on the flutter speed of a slender wing. The deformed shape of the wing at flutter condition is a coupled bending-torsion as shown in Figure 5.11 below. This shows agreement with classic flutter theory, which requires a coupling of two or more vibration modes for flutter to occur [60].

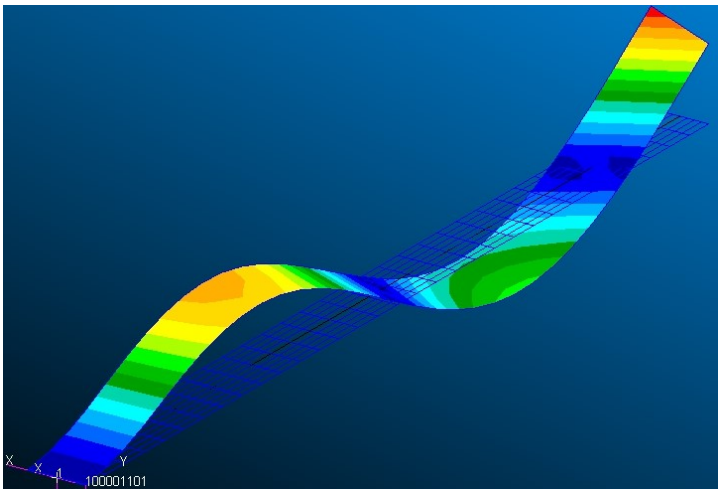

Figure 5.11: PATRAN screen-shot of the critical aeroelastic mode (mode 4) at the nonlinear V_f for 2° AOA, sea level, gravity 'off'

5.4. The Capricious Second Mode

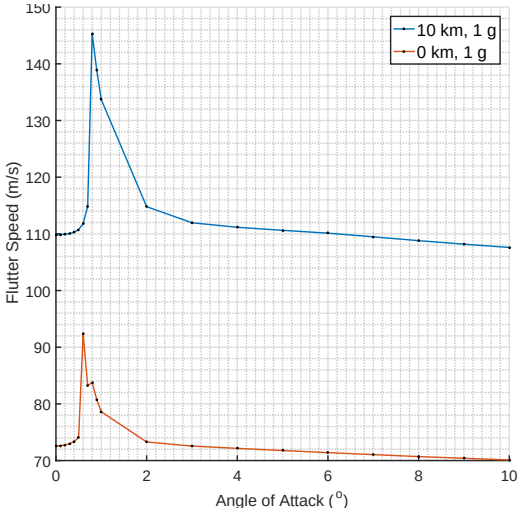

Figure 5.12: Flutter speed vs AOA with mode 2 as the critical mode

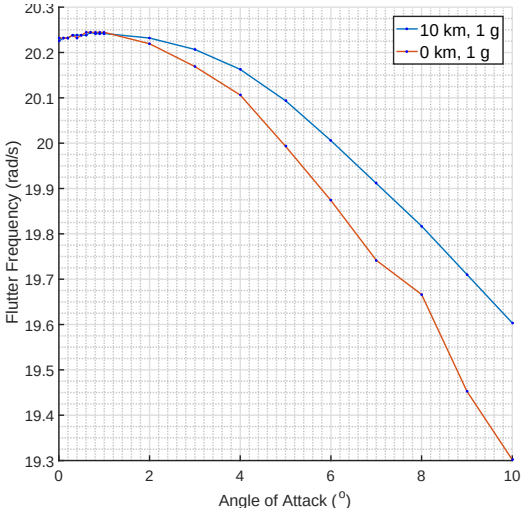

Figure 5.13: Flutter frequency vs AOA with mode 2 as the critical mode

Almost all the plots in this chapter regarding the effects of geometric nonlinearities on aeroelastic behaviour lie in the range of $60 - 90m/s$. This is because of the way the nonlinear flutter solution was set up. The velocity range for which the iterative process was run was increased incrementally. The results for the analysis at sea level showed mode 2 to be the critical mode at about $90m/s$. The flutter speeds and frequencies derived using this mode are shown in Figures 5.12 and 5.13.

A 'spike' in the flutter speed is seen at about $0.6°$, when the aerodynamic loads overcome the gravity loads and the wing tip deflection changes from negative to positive. This reflected results shown in literature ("Fig. 2 Variation of flutter speed with angle of attack", Patil et al. [86]). Thus they were taken at face value. However, a further look showed that this mode is an edge-wise bending mode. It consists of in-plane structural bending which translates to the torsion of the lifting panel. Because drag effects are not included in DLM [95], this mode is always undamped. Thus, its behaviour cannot be considered reliable. Figure 5.14 shows how little the shape of this mode varies with a change in load, especially in comparison to modes 1 and 4 (Figures 5.6, 5.7). This further supports the previous inference. The velocity range for flutter analysis was expanded until the actual flutter mode was found.

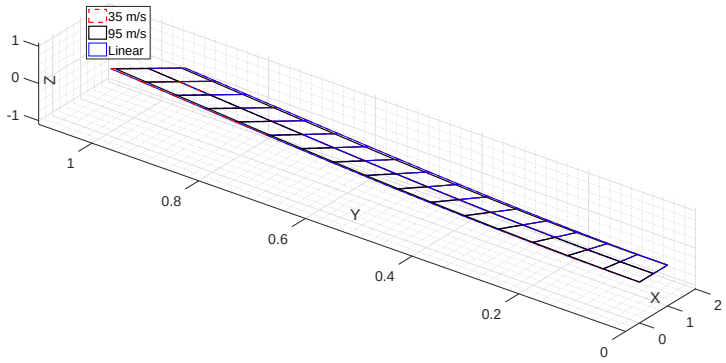

Figure 5.14: Change in normalised shape of mode 2 with airspeed at 5° AOA, sea level

5.5. Conclusions

In the previous chapters, procedures for nonlinear static aeroelastic analysis and flutter analysis with nonlinear modes were described and validated for the case of a simple HAR wing. The results of this exercise were two-fold. First, the capability of commercially available FEA software to successfully predict nonlinear aeroelastic behaviour was demonstrated. Second, it was shown that nonlinear geometric behaviour has a significant impact on the aeroelastic deformation, natural frequencies and the flutter stability of slender, flexible wings. It was observed that the stress in such wings can affect their modal characteristics in a counter-intuitive fashion, leading to increased stability at high deformations. However, such behaviour is not a given. The effect the stress state has on the static and dynamic stability of a wing would depend on the structural properties of the wing in question.

The record would not be complete without highlighting certain limitations of the analysis method. The nonlinear structural model cannot, as of now, be directly used in the flutter module. Static nonlinear equilibrium states have to be derived separately and imported. This makes the flutter analysis a linear dynamic analysis about a nonlinear static condition. Because of this, the wing oscillation is limited to small amplitudes. True, geometrically nonlinear flutter with large amplitude oscillations cannot be analysed. The method in its current form can only analyse cantilevered wings. This limits the vertical load factor to 1G. Also, since the wing is not free to undergo any RBM, phenomena involving RBM-elastic interaction, like antisymmetric flutter modes cannot be captured [34]. The use of a linear aerodynamic model limits the validity of results to low Mach numbers (incompressible flows). To capture the effects of drag, shock or compressibility, correction factors are required. This, in turn, would require hi-fidelity CFD simulations or experiments. The ability of this method to incorporate material nonlinearities has also not been explored.

6

Recommendations and Future Work

The current nonlinear iterative analysis takes about 100 seconds to converge for one static aeroelastic load case (one AOA, speed and altitude). Analysing 27-30 velocities at a fixed AOA and altitude takes about 40 minutes. Another 20 minutes are required for flutter analysis at each velocity and for collating the flutter summary tables into a $V - g$ plot. The time take for static aeroelastic and flutter analysis of all these velocities at 9 angles of attack is around 8 hours. Ironically, the time taken to run the analysis increases non-linearly with the number of load cases. The time taken to analyse each successive load case increases as MATLAB and NASTRAN temporary memory becomes loaded with variables of the previous iteration. A look at MATLAB's profiler output shows that a major portion of this time is taken in exporting data from NASTRAN's text output files to MATLAB variables and using those variables to create a new direct text input file for NASTRAN. If the algorithm for this analysis can be implemented using the Direct Matrix Abstraction Program (DMAP), the output for one iteration could be transferred to the input variables for the next iteration internally in NASTRAN. This would eliminate a major chunk of the processing time. The accuracy of the flutter solution improves if the velocities for successive load cases are spaced close to each other. This time could be used to analyse more load cases, in order to provide better interpolation for the flutter results. Implementing the analysis method in DMAP would also allow the aerodynamic loads to be added in increments. The converged nonlinear condition for each increment could be used as the starting point for the next increment, as is the case in the nonlinear static solver. The solutions for one load case could be used as a starting point for the next load case, saving a lot of processing time. Castellani et al. [17] have implemented a similar procedure for nonlinear aeroelastic trim using DMAP.

Another recommendation is to add the capability to analyse aircraft RBM to the present analysis. The interaction between RBM and elastic deformation greatly affects the aeroelastic behaviour in flexible aircraft. This thesis was unable to incorporate this effect due to time constraints. As mentioned at the conclusion of Chapter 5, this would also allow load factors higher than 1-G to be analysed. The effect of nonlinear static preload on flutter has been shown to be significant. Extending this approach to analyse other dynamic aeroelastic phenomena like the response to gust loads, ejection of external stores and payload release in ALO platforms would be a worthwhile undertaking. It would be interesting to apply this analysis to a full, unconventional aircraft like the SratoLaunch and compare the results with hi-fidelity analyses and actual flight data. This would provide a more complete idea about the accuracy of the analysis method and give more reliable information to designers selecting safety margins.

Bibliography

[1] Frederico Afonso, Gonçalo Leal, José Vale, Éder Oliveira, Fernando Lau, and Afzal Suleman. Linear vs non-linear aeroelastic analysis of high aspect-ratio wings. In *Congress of Numerical Methods in Engineering, 29 Jun.-02 Jul. 2015*, volume 29. APMTAC, 2015.

[2] Frederico Afonso, José Vale, Éder Oliveira, Fernando Lau, and Afzal Suleman. A review on non-linear aeroelasticity of high aspect-ratio wings. *Progress in Aerospace Sciences*, 89:40–57, 2017. ISSN 03760421. doi: 10.1016/j.paerosci.2016.12.004.

[3] Edward Albano and William P. Rodden. A doublet-lattice method for calculating lift distributions on oscillating surfaces in subsonic flows. *AIAA Journal*, 7(2):279–285, 1969. ISSN 0001-1452. doi: 10.2514/3.5086. URL https://arc.aiaa.org/doi/abs/10.2514/3.5086.

[4] Timothy Allen, Bradley Sexton, and Matthew J. Scott. SUGAR truss braced wing full scale aeroelastic analysis and dynamically scaled wind tunnel model development. In *56th AIAA/ASCE/AHS/ASC Structures, Structural Dynamics, and Materials Conference*, page 1171, 2015.

[5] Andrea Arena, Walter Lacarbonara, and Pier Marzocca. Nonlinear aeroelastic formulation and postflutter analysis of flexible high-aspect-ratio wings. *Journal of Aircraft*, 50(6):1748–1764, 2013. ISSN 0021-8669. doi: 10.2514/1.C032145. URL https://doi.org/10.2514/1.C032145.

[6] Holt Ashley. Aeroelasticity. *Applied Mechanics Reviews*, 23(2):119–129, 1970.

[7] Holt Ashley. *"Update to" Aeroelasticity [AMR 23 (1970): 119-129]*, volume vii, book section 23, pages 117–125. ASME, New York, N.Y., 1986. URL //catalog.hathitrust.org/Record/005802068http://hdl.handle.net/2027/wu.89012624813.

[8] Robert E. Bartels, Robert C. Scott, Timothy Allen, and Bradley Sexton. Aeroelastic analysis of SUGAR truss-braced wing wind-tunnel model using FUN3D and a nonlinear structural model. In *56th AIAA/ASCE/AHS/ASC Structures, Structural Dynamics, and Materials Conference, 05-09 Jan.* AIAA, 2015. doi: 10.2514/6.2015-1174. URL https://arc.aiaa.org/doi/pdf/10.2514/6.2015-1174.

[9] Olivier A. Bauchau, Carlo L. Bottasso, and Yuri G Nikishkov. Modeling rotorcraft dynamics with finite element multibody procedures. *Mathematical and Computer Modelling*, 33(10-11):1113–1137, 2001. ISSN 0895-7177.

[10] Philip Beran, JiYoung Hur, Richard Snyder, Daniel Strong, Dean Bryson, and Thomas W. Strganac. Static nonlinear aeroelastic analysis of a blended wing body, AIAA-2005-1944. In *46th AIAA/ ASME/ ASCE/ AHS/ ASC Structures, Structural Dynamics and Materials Conference, 18-21 Apr.* AIAA, 2005. doi: 10.2514/6.2005-1944.

[11] Samarth Bhasin. An interface for aeroelastic analysis of joined wing configurations including structural nonlinearities. Master's thesis, San Diego State University, 2011.

[12] Raymond L. Bisplinghoff, Holt Ashley, and Robert L. Halfman. *Aeroelasticity*. Dover Publications, 1996. ISBN 9780486691893. URL https://books.google.nl/books?id=jtqDQ2nTvvcC.

[13] Vanessa L. Bond, Robert A. Canfield, Afzal Suleman, and Maxwell Blair. Aeroelastic scaling of a joined wing for nonlinear geometric stiffness. *AIAA Journal*, 50(3):513–522, 2012. ISSN 0001-1452 1533-385X. doi: 10.2514/1.41139.

[14] William N. Boyd. *Effect of Chordwise Forces and Deformations and Deformation due to Steady Lift on Wing Flutter*. PhD thesis, Stanford University, 1977. URL https://ntrs.nasa.gov/search.jsp?R=19780021167.

[15] Eric Lee Brown. *Integrated strain actuation in aircraft with highly flexible composite wings*. PhD thesis, Massachusetts Institute of Technology, 2003. URL http://hdl.handle.net/1721.1/8001.

[16] Edward Burnett, Chris Atkinson, Jeff Beranek, Brian Sibbitt, Brian Holm-Hansen, and Leland Nicolai. NDOF simulation model for flight control development with flight test correlation, AIAA 2010-7780. In *AIAA Modeling and Simulation Technologies Conference, 2-5 Aug.* AIAA, 2010. doi: 10.2514/6.2010-7780.

[17] Michele Castellani, Jonathan E. Cooper, and Yves Lemmens. Nonlinear static aeroelasticity of high-aspect-ratio-wing aircraft by finite element and multibody methods. *Journal of Aircraft*, 54 (2):548–560, 2017. ISSN 0021-8669 1533-3868. doi: 10.2514/1.C033825.

[18] Luca Cavagna, Sergio Ricci, and Luca Riccobene. A fast tool for structural sizing, aeroelastic analysis and optimization in aircraft conceptual design, AIAA 2009-2571. In *50th AIAA/ ASME/ ASCE/ AHS/ ASC Structures, Structural Dynamics, and Materials Conference, 4-7 May*. AIAA, 2009. doi: 10.2514/6.2009-2571.

[19] Luca Cavagna, Pierangelo Masarati, and Giuseppe Quaranta. Coupled multibody/computational fluid dynamics simulation of maneuvering flexible aircraft. *Journal of Aircraft*, 48(1):92–106, 2011. ISSN 0021-8669 1533-3868. doi: 10.2514/1.C000253.

[20] Jiri Cecrdle and Ondrej Vich. Eigenvalue and flutter sensitivity analysis of airliner wing. In *27th Congress of the International Council of the Aeronautical Sciences*. ICAS 2012, 2012.

[21] Carlos E. S. Cesnik and Eric Lee Brown. Modeling of high aspect ratio active flexible wings for roll control, AIAA 2002-1719. In *43rd AIAA/ ASME/ ASCE/ AHS/ ASC Structures, Structural Dynamics, and Materials Conference, 22-25 Apr.* AIAA, 2002. doi: 10.2514/6.2002-1719.

[22] Carlos E. S. Cesnik and Eric Lee Brown. Active warping control of a joined wing/tail airplane configuration, AIAA 2003-1715. In *44th AIAA/ ASME/ ASCE/ AHS/ ASC Structures, Structural Dynamics, and Materials Conference, 07-10 Apr.* American Insititute of Aeronautics and Astronautics, 2003. doi: 10.2514/6.2003-1715.

[23] Carlos E. S. Cesnik and Dewey H. Hodges. VABS: a new concept for composite rotor blade cross□-sectional modeling. *Journal of the American helicopter society*, 42(1):27–38, 1997. ISSN 2161-6027. doi: 10.4050/JAHS.42.27. URL https://doi.org/10.4050/JAHS.42.27.

[24] Carlos E. S. Cesnik and Miguel Ortega-Morales. Active beam cross-sectional modeling. *Journal of Intelligent Material Systems and Structures*, 12(7):483–496, 2001. doi: 10.1177/10453890122145285. URL http://journals.sagepub.com/doi/abs/10.1177/10453890122145285.

[25] Carlos E. S. Cesnik and Rafael Palacios. Modeling piezocomposite actuators embedded in slender structures, AIAA 2003-1803. In *44th AIAA/ ASME/ ASCE/ AHS/ ASC Structures, Structural Dynamics, and Materials Conference, 07-10 Apr.* AIAA, 2003. doi: 10.2514/6.2003-1803. URL https://arc.aiaa.org/doi/abs/10.2514/6.2003-1803.

[26] Carlos E. S. Cesnik and Sangjoon Shin. On the modeling of integrally actuated helicopter blades. *International Journal of Solids and Structures*, 38(10):1765–1789, 2001. ISSN 0020-7683. doi: 10.1016/S0020-7683(00)00135-9. URL http://www.sciencedirect.com/science/article/pii/S0020768300001359.

[27] Carlos E. S. Cesnik and Weihua Su. Nonlinear aeroelastic behavior of fully flexible slender vehicles. In *International Forum on Aeroelasticity and Structural Dynamics*, 2005.

[28] Carlos E. S. Cesnik and Weihua Su. Nonlinear aeroelastic modeling and analysis of fully flexible aircraft, AIAA 2005-2169. In *46th AIAA/ ASME/ ASCE/ AHS/ ASC Structures, Structural Dynamics and Materials Conference, 18-21 Apr.* AIAA, 2005. doi: 10.2514/6.2005-2169. URL https://arc.aiaa.org/doi/pdf/10.2514/6.2005-2169.

[29] Carlos E. S. Cesnik, Dewey H. Hodges, and Vladislav G. Sutyrin. Cross-sectional analysis of composite beams including large initial twist and curvature effects. *AIAA Journal*, 34(9):1913–1920, 1996. ISSN 0001-1452 1533-385X. doi: 10.2514/3.13325. URL https://arc.aiaa.org/doi/pdf/10.2514/3.13325.

[30] Carlos E. S. Cesnik, Dewey H. Hodges, and Vladislav G. Sutyrin. Refined theory of composite beams: The role of short-wavelength extrapolation. *International Journal of Solids and Structures*, 33(10):1387–1408, 1996. ISSN 0020-7683. doi: 10.1016/0020-7683(95)00109-3. URL http://www.sciencedirect.com/science/article/pii/0020768395001093.

[31] C. S. Chang, Dewey H. Hodges, and Mayuresh J. Patil. Flight dynamics of highly flexible aircraft. *Journal of Aircraft*, 45(2):538–545, 2008. ISSN 0021-8669 1533-3868. doi: 10.2514/1.30890. URL https://arc.aiaa.org/doi/pdf/10.2514/1.30890.

[32] Tao Cheng. Structural dynamics modeling of helicopter blades for computational aeroelasticity. Master's thesis, Massachusetts Institute of Technology, 2002.

[33] John M. Coggin, Rakesh K. Kapania, Joseph A. Schetz, H. Vijayakumari, and Wei Zhao. Nonlinear aeroelastic analysis of a truss based wing aircraft. In *55th AIAA/ ASME/ ASCE/ AHS/ ASC Structures, Structural Dynamics, and Materials Conference*, 2014. doi: 10.2514/6.2014-0335.

[34] A. R. Collar. The expanding domain of aeroelasticity. *The Journal of the Royal Aeronautical Society*, 50(428):613–636, 1946. ISSN 0368-3931. doi: 10.1017/S0368393100120358. URL https://doi.org/10.1017/S0368393100120358.

[35] J. D. Connelly and R. L. Huston. The dynamics of flexible multibody systems: A finite segment approach-I. theoretical aspects. *Computers & Structures*, 50(2):255–258, 1994. ISSN 0045-7949. doi: 10.1016/0045-7949(94)90300-X. URL http://www.sciencedirect.com/science/article/pii/004579499490300X.

[36] Luciano Demasi and Eli Livne. Exploratory studies of joined-wing aeroelasticity, AIAA 2005-2172. In *46th AIAA/ ASME/ ASCE/ AHS/ ASC Structures, Structural Dynamics and Materials Conference, 18-21 Apr.* AIAA, 2005. doi: 10.2514/6.2005-2172.

[37] Luciano Demasi and Eli Livne. The structural order reduction challenge in the case of geometrically nonlinear joined-wing configurations, AIAA 2007-2052. In *48th AIAA/ ASME/ ASCE/ AHS/*

ASC Structures, Structural Dynamics, and Materials Conference, 23-26 Apr. AIAA, 2007. doi: 10.2514/6.2007-2052.

[38] Luciano Demasi, Rauno Cavallaro, and Alan Márquez Razón. Postcritical analysis of prandtlplane joined-wing configurations. *AIAA Journal*, 51(1):161–177, 2012. ISSN 0001-1452. doi: 10.2514/1.J051700. URL https://doi.org/10.2514/1.J051700.

[39] Earl H. Dowell. *Nonlinear Aeroelasticity*, volume Vol. 5-Structural Dynamics and Aeroelasticity, book section 4, pages 213–239. ASME, New York, 1993.

[40] Earl H. Dowell, John W. Edwards, and Thomas W. Strganac. Nonlinear aeroelasticity. *Journal of Aircraft*, 40(5):857–874, 2003. ISSN 0021-8669. doi: 10.2514/2.6876. URL https://doi.org/10.2514/2.6876.

[41] Mark Drela. Integrated simulation model for preliminary aerodynamic, structural, and control-law design of aircraft. In *40th Structures, Structural Dynamics, and Materials Conference and Exhibit*, 1999. doi: 10.2514/6.1999-1394.

[42] John W. Edwards. *Computational Aeroelasticity*, volume Vol. 5-Structural Dynamics and Aeroelasticity, book section 7, pages 393–436. ASME, New York, 1993.

[43] John W. Edwards. Transonic shock oscillations and wing flutter calculated with an interactive boundary layer coupling method. In *349th EUROMECH-Colloquium: Simulation of Fluid-Structure Interaction in Aeronautics, 16 - 19 Sep.*, 1996. URL https://ntrs.nasa.gov/search.jsp?R=19960054470.

[44] Stan Ferguson, Adrian Viisoreanu, Scott Schwimley, and Gerry Miller. Integrated nonlinear aerodynamic-structural tool for external loads development, AIAA 2007-6382. In *AIAA Atmospheric Flight Mechanics Conference and Exhibit, 20-23 Aug.* AIAA, 2007. doi: 10.2514/6.2007-6382.

[45] Antonio Filippone. Data and performances of selected aircraft and rotorcraft. *Progress in Aerospace Sciences*, 36(8):629–654, 2000. ISSN 0376-0421. doi: 10.1016/S0376-0421(00)00011-7. URL http://www.sciencedirect.com/science/article/pii/S0376042100000117.

[46] Peretz P. Friedmann. Renaissance of aeroelasticity and its future. *Journal of Aircraft*, 36(1):105–121, 1999. ISSN 0021-8669 1533-3868. doi: 10.2514/2.2418.

[47] Joseph A. Garcia. Numerical investigation of nonlinear aeroelastic effects on flexible high-aspect-ratio wings. *Journal of Aircraft*, 42(4):1025–1036, 2005. ISSN 0021-8669 1533-3868. doi: 10.2514/1.6544.

[48] I. E. Garrick and Wilmer H. Reed III. Historical development of aircraft flutter. *Journal of Aircraft*, 18(11):897–912, 1981. ISSN 0021-8669. doi: 10.2514/3.57579. URL https://doi.org/10.2514/3.57579.

[49] Gian Luca Ghiringhelli, Pierangelo Masarati, and Paolo Mantegazza. Multibody implementation of finite volume c beams. *AIAA Journal*, 38(1):131–138, 2000. ISSN 0001-1452. doi: 10.2514/2.933. URL https://doi.org/10.2514/2.933.

[50] J. P. Giesing, T. P. Kalman, and William P. Rodden. Correction factor techniques for improving aerodynamic prediction methods. Report NASA-CR-144967, NASA, 1976. URL https://ntrs.nasa.gov/search.jsp?R=19760016071.

[51] Antônio B. Guimarães Neto, Roberto G. A. Silva, Pedro Paglione, and Flávio J. Silvestre. Formulation of the flight dynamics of flexible aircraft using general body axes. *AIAA Journal*, 54(11):3516–3534, 2016. ISSN 0001-1452 1533-385X. doi: 10.2514/1.J054752. URL https://arc.aiaa.org/doi/pdf/10.2514/1.J054752.

[52] Mohammad Yazdi Harmin and Jonathan E. Cooper. Aeroelastic behaviour of a wing including geometric nonlinearities. *The Aeronautical Journal*, 115(1174):767–777, 2011. ISSN 0001-9240. doi: 10.1017/S0001924000006515. URL https://doi.org/10.1017/S0001924000006515.

[53] Peter M. Hartwich, Steven K. Dobbs, Alan E. Arslan, and Suk C. Kim. Navier-stokes computations of limit-cycle oscillations for a B-1-like configuration. *Journal of Aircraft*, 38(2):239–247, 2001. ISSN 0021-8669 1533-3868. doi: 10.2514/2.2781.

[54] Sven G. Hedman. Vortex lattice method for calculation of quasi steady state loadings on thin elastic wings in subsonic flow. Report FFA-105, AERONAUTICAL RESEARCH INST OF SWEDEN, STOCKHOLM, 1966. URL http://www.dtic.mil/dtic/tr/fulltext/u2/687165.pdf.

[55] Dewey H. Hodges. A mixed variational formulation based on exact intrinsic equations for dynamics of moving beams. *International Journal of Solids and Structures*, 26(11):1253–1273, 1990. ISSN 00207683. doi: 10.1016/0020-7683(90)90060-9. URL https://doi.org/10.1016/0020-7683(90)90060-9.

[56] Dewey H. Hodges. Geometrically exact, intrinsic theory for dynamics of curved and twisted anisotropic beams. *AIAA Journal*, 41(6):1131–1137, 2003. ISSN 0001-1452. doi: 10.2514/2.2054. URL https://doi.org/10.2514/2.2054.

[57] Dewey H. Hodges and Earl H. Dowell. Nonlinear equations of motion for the elastic bending and torsion of twisted nonuniform rotor blades. Report NASA-TN-D-7818, NASA Ames Research Center; Moffett Field, CA, United States, 1974. URL https://ntrs.nasa.gov/search.jsp?R=19750005242.

[58] Dewey H. Hodges and Robert A. Ormiston. Stability of elastic bending and torsion of uniform cantilever rotor blades in hover with variable structural coupling. Report NASA-TN-D-8192, NASA Ames Research Center; Moffett Field, CA, United States, 1976. URL https://ntrs.nasa.gov/search.jsp?R=19760014074.

[59] Chris Howcroft, Dario Calderon, Luke Lambert, Michele Castellani, Jonathan E. Cooper, Mark H. Lowenberg, and Simon Neild. Aeroelastic modelling of highly flexible wings. In *15th Dynamics Specialists Conference, AIAA Sci Tech Forum*, San Diego, California, USA, 2016. AIAA. doi: 10.2514/6.2016-1798.

[60] S. J. Hulsoff. *Course AE4930 Aeroelasticity, November 2011 (Version 11.1)*. Faculty of Aerospace Engineering, TU Delft, 2011.

[61] Justin W Jaworski. *Nonlinear aeroelastic analysis of flexible high aspect ratio wings including correlation with experiment (Abstract)*. PhD thesis, Duke University, 2009.

[62] Jessica Jones and Carlos E. S. Cesnik. Nonlinear aeroelastic analysis of the x-56 multi-utility aeroelastic demonstrator. In *15th Dynamics Specialists Conference, 04-08 Jan. 2016*. AIAA, 2016. doi: 10.2514/6.2016-1799.

[63] Y. I. Kim, G. J. Park, R. M. Kolonay, Maxwell Blair, and Robert A. Canfield. Nonlinear response structural optimization of a joined wing using equivalent loads. *AIAA Journal*, 46(11):2703–2713,

2008. ISSN 0001-1452. doi: 10.2514/1.33428. URL https://doi.org/10.2514/1.33428.

[64] Wolf R. Krüger. Multibody dynamics for the coupling of aeroelasticity and flight mechanics of highly flexible structures, IFASD-2007-107. In *International Forum on Aeroelasticity and Structural Dynamics, June 2007*, 2007.

[65] Wolf R. Krüger and Martin Spieck. Aeroelastic effects in multibody dynamics. *Vehicle System Dynamics*, 41(5):383–399, 2004. ISSN 0042-3114. doi: 10.1080/00423110412331300345. URL https://doi.org/10.1080/00423110412331300345.

[66] Robert S. Lahey, Mark P. Miller, and Michael Reymond. *MSC/ NASTRAN reference manual, version 68*. MacNeal-Schwendler Corporation, 1994.

[67] H. A. Lee, Y. I. Kim, G. J. Park, R. M. Kolonay, Maxwell Blair, and Robert A. Canfield. Structural optimization of a joined wing using equivalent static loads. *Journal of Aircraft*, 44(4):1302–1308, 2007. ISSN 0021-8669 1533-3868. doi: 10.2514/1.26869. URL https://arc.aiaa.org/doi/pdf/10.2514/1.26869.

[68] Sang H Lee. *MSC/NASTRAN Handbook for nonlinear analysis: version 67*. MacNeal-Schwendler Corporation, 1992.

[69] Eli Livne. Future of airplane aeroelasticity. *Journal of Aircraft*, 40(6):1066–1092, 2003. ISSN 0021-8669 1533-3868. doi: 10.2514/2.7218.

[70] Eli Livne and Terrence A. Weisshaar. Aeroelasticity of nonconventional airplane configurations-past and future. *Journal of Aircraft*, 40(6):1047–1065, 2003. ISSN 0021-8669 1533-3868. doi: 10.2514/2.7217.

[71] Michael Love, P. Zink, Paul Wieselmann, and Harold Youngren. Body freedom flutter of high aspect ratio flying wings, AIAA 2005-1947. In *46th AIAA/ ASME/ ASCE/ AHS/ ASC Structures, Structural Dynamics and Materials Conference, 18-21 Apr.* AIAA, 2005. doi: 10.2514/6.2005-1947. URL https://arc.aiaa.org/doi/pdf/10.2514/6.2005-1947.

[72] Chuh Mei and Jr. Rogers, James L. NASTRAN nonlinear vibration analysis of beam and frame structures. In *4th NASTRAN Users' Colloquium; 9-11 Sep. 1975*, page 26. NASA, 1975. URL https://ntrs.nasa.gov/search.jsp?R=19750023427.

[73] Haris Hameed Mian, Gang Wang, and Zheng-Yin Ye. Numerical investigation of structural geometric nonlinearity effect in high-aspect-ratio wing using cfd/ csd coupled approach. *Journal of Fluids and Structures*, 49:186–201, 2014. ISSN 0889-9746. doi: 10.1016/j.jfluidstructs.2014.04.011. URL http://www.sciencedirect.com/science/article/pii/S0889974614000875.

[74] Scott Geoffrey Moon. Aero-structural optimization of divergence-critical wings. Master's thesis, University of Toronto, 2009. URL http://hdl.handle.net/1807/18911.

[75] Vivek Mukhopadhyay. Blended wing body (BWB) fuselage structural design for weight reduction, AIAA 2005-2349. In *46th AIAA/ ASME/ ASCE/ AHS/ ASC Structures, Structural Dynamics and Materials Conference, 18-21 Apr.* AIAA, 2005. doi: 10.2514/6.2005-2349. URL https://arc.aiaa.org/doi/pdf/10.2514/6.2005-2349.

[76] Nhan Nguyen and Ilhan Tuzcu. Flight dynamics of flexible aircraft with aeroelastic and inertial force interactions, AIAA 2009-6045. In *AIAA Atmospheric Flight Mechanics Conference, 10-13 Aug.* American Institute of Aeronautics and Astronautics„ 2009. doi: 10.2514/6.2009-6045.

[77] Rafael Palacios and Carlos E. S. Cesnik. Static nonlinear aeroelasticity of flexible slender wings in compressible flow, AIAA 2005-1945. In *46th AIAA/ ASME/ ASCE/ AHS/ ASC Structures, Structural Dynamics and Materials Conference, 18-21 Apr.* AIAA, 2005. doi: 10.2514/6.2005-1945. URL https://arc.aiaa.org/doi/pdf/10.2514/6.2005-1945.

[78] Rafael Palacios, H. Climent, A. Karlsson, and B. Winzell. *Assessment of Strategies for Correcting Linear Unsteady Aerodynamics Using CFD or Test Results, IFASD-2001-074*, volume 1, pages 195–210. AIAA, Madrid, 2001. ISBN 9788493137557.

[79] Rafael Palacios, Joseba Murua, and Robert Cook. Structural and aerodynamic models in nonlinear flight dynamics of very flexible aircraft. *AIAA Journal*, 48(11):2648–2659, 2010. ISSN 0001-1452-1533-385X. doi: 10.2514/1.J050513. URL https://arc-aiaa-org.tudelft.idm.oclc.org/doi/pdf/10.2514/1.J050513.

[80] Mayuresh Patil, Dewey Hodges, and Carlos Cesnik. Nonlinear aeroelastic analysis of aircraft with high-aspect-ratio wings. In *39th AIAA/ ASME/ ASCE/ AHS/ ASC Structures, Structural Dynamics, and Materials Conference and Exhibit*. AIAA, 1998. doi: 10.2514/6.1998-1955. URL https://doi.org/10.2514/6.1998-1955.

[81] Mayuresh J. Patil. *Nonlinear aeroelastic analysis, flight dynamics, and control of a complete aircraft*. PhD thesis, Georgia Institute of Technology, 1999.

[82] Mayuresh J. Patil and Dewey H. Hodges. Flight dynamics of highly flexible flying wings. *Journal of Aircraft*, 43(6):1790–1799, 2006. ISSN 0021-8669 1533-3868. doi: 10.2514/1.17640. URL https://arc.aiaa.org/doi/pdf/10.2514/1.17640.

[83] Mayuresh J. Patil, Dewey H. Hodges, and Carlos E. S. Cesnik. *Characterizing the effects of geometrical nonlinearities on aeroelastic behavior of high-aspect ratio wings*, volume 2, pages 501–510. AIAA, 1999. ISBN 0191-7811.

[84] Mayuresh J. Patil, Dewey H. Hodges, and Carlos E. S. Cesnik. Limit cycle oscillations in high-aspect-ratio wings, AIAA 99-1464. In *40th Structures, Structural Dynamics, and Materials Conference and Exhibit 12-15 Apr.* AIAA, 1999. doi: 10.2514/6.1999-1464. URL https://arc.aiaa.org/doi/pdf/10.2514/6.1999-1464.

[85] Mayuresh J. Patil, Dewey H. Hodges, and Carlos E. S. Cesnik. Nonlinear aeroelastic analysis of complete aircraft in subsonic flow. *Journal of Aircraft*, 37(5):753–760, 2000. ISSN 0021-8669 1533-3868. doi: 10.2514/2.2685. URL https://arc.aiaa.org/doi/pdfplus/10.2514/2.2685.

[86] Mayuresh J. Patil, Dewey H. Hodges, and Carlos E. S. Cesnik. Nonlinear aeroelasticity and flight dynamics of high-altitude long-endurance aircraft. *Journal of Aircraft*, 38(1):88–94, 2001. ISSN 0021-8669 1533-3868. doi: 10.2514/2.2738. URL https://arc.aiaa.org/doi/pdf/10.2514/2.2738.

[87] Pedro Pereira, Luis Almeida, Afzal Suleman, Vanessa L. Bond, Robert A. Canfield, and Maxwell Blair. Aeroelastic scaling and optimization of a joined-wing aircraft concept, AIAA 2007-1889. In *48th AIAA/ ASME/ ASCE/ AHS/ ASC Structures, Structural Dynamics, and Materials Conference, 23-26 Apr.* AIAA, 2007. doi: 10.2514/6.2007-1889. URL https://arc.aiaa.org/doi/pdf/10.2514/6.2007-1889.

[88] David A. Peters and Mark James Johnson. *Finite-State Airloads for Deformable Airfoils on Fixed and Rotating Wings*, volume 44 of *ASME, Aerospace Division (Publication)*, pages 1–28. ASME, New York, USA, 1994. ISBN 079181453X 07334230 (ISSN).

[89] Augustin Petre and Holt Ashley. Drag effects on wing flutter. *Journal of Aircraft*, 13(10):755–763, 1976. ISSN 0021-8669 1533-3868. doi: 10.2514/3.58707. URL https://arc-aiaa-org.tudelft.idm.oclc.org/doi/10.2514/3.58707.

[90] Torrey Radcliffe and Carlos E. S. Cesnik. Aeroelastic response of multi-segmented hinged wings, AIAA 2001-1371. In *19th AIAA Applied Aerodynamics Conference, 11-14 Jun.* AIAA, 2001. doi: 10.2514/6.2001-1371. URL https://arc.aiaa.org/doi/pdf/10.2514/6.2001-1371.

[91] S. Ragon and Z. Gurdal. Effects of geometric nonlinearities on the response of optimized boxbeam structures, AIAA 93-1412. In *34th AI AAIASME/ASCE/AHS/ASC Structures, Structural Dynamics and Materials Conference, 19-22 Apr.* AIAA, 1993. doi: 10.2514/6.1993-1412. URL https://arc.aiaa.org/doi/pdf/10.2514/6.1993-1412.

[92] S. Ragon, Z. Guerdal, and Jr. Starnes, J. Optimization of composite box-beam structures including the effects of subcomponent interaction, AIAA 94-1410-cp. In *35th Structures, Structural Dynamics, and Materials Conference, 18-20 Apr.* AIAA, 1994. doi: 10.2514/6.1994-1410. URL https://arc.aiaa.org/doi/pdf/10.2514/6.1994-1410.

[93] Mario H. Rheinfurth and Fredrick W. Swift. A new approach to the explanation of the flutter mechanism. Report NASA-TN-D-3125, NASA, 1966. URL https://ntrs.nasa.gov/search.jsp?R=19660006195.

[94] Cristina Riso, Franco Mastroddi, and Carlos E. S. Cesnik. Coupled flight dynamics and aeroelasticity of very flexible aircraft based on commercial finite element solvers. In *2018 AIAA/ASCE/AHS/ASC Structures, Structural Dynamics, and Materials Conference*, 2018. doi: 10.2514/6.2018-1685.

[95] William P. Rodden and Erwin H. Johnson. *MSC/NASTRAN aeroelastic analysis: user's guide; Version 68*. MacNeal-Schwendler Corporation, 1994.

[96] M. A. A. Salman, Mostafa S. A. ElSayed, and Denis Walch. Structural nonlinearities and their impact on the fidelity of critical steady maneuver loads and trimming configuration of very flexible airframes. *Journal of Aeroelasticity and Structural Dynamics*, 6(1):1–20, 2018. doi: 10.3293/asdj.2018.45.

[97] Francesco Saltari, Cristina Riso, Guido De Matteis, and Franco Mastroddi. Finite-element-based modeling for flight dynamics and aeroelasticity of flexible aircraft. *Journal of Aircraft*, 54(6):2350–2366, 2017. ISSN 0021-8669 1533-3868. doi: 10.2514/1.C034159.

[98] David K. Schmidt. Stability augmentation and active flutter suppression of a flexible flying-wing drone. *Journal of Guidance, Control, and Dynamics*, 39(3):409–422, 2016. ISSN 0731-5090 1533-3884. doi: 10.2514/1.G001484. URL https://arc.aiaa.org/doi/pdf/10.2514/1.G001484.

[99] David K. Schmidt. MATLAB-based flight-dynamics and flutter modeling of a flexible flying-wing research drone. *Journal of Aircraft*, 53(4):1045–1055, 2016. ISSN 0021-8669 1533-3868. doi: 10.2514/1.C033539.

[100] David K. Schmidt and David L. Raney. Modeling and simulation of flexible flight vehicles. *Journal of Guidance, Control, and Dynamics*, 24(3):539–546, 2001. ISSN 0731-5090 1533-3884. doi: 10.2514/2.4744.

[101] David M. Schuster, D. D. Liu, and Lawerence J. Huttsell. Computational aeroelasticity: Success, progress, challenge. *Journal of Aircraft*, 40(5):843–856, 2003. ISSN 0021-8669. doi: 10.2514/2.6875. URL https://doi.org/10.2514/2.6875.

[102] Robert G Schwendler, Richard H MacNeal, and Computer Engineering Associates Inc. Optimum structural representation in aeroelastic analyses. Report ASD-TR-61-680, Flight Control Laboratory, Wright-Patterson AFB, 1962. URL http://www.dtic.mil/dtic/tr/fulltext/u2/277468.pdf.

[103] A.A. Shabana. *Dynamics of Multibody Systems*. Cambridge University Press, 2013. ISBN 9781107042650. URL https://books.google.nl/books?id=DWRsAAAAQBAJ.

[104] Xiaoyang Shang. *Aeroelastic stability of composite hingeless rotors with finite-state unsteady aerodynamics*. PhD thesis, Georgia Institute of Technology, 1995. URL http://hdl.handle.net/1853/12543.

[105] Christopher M. Shearer and Carlos E. S. Cesnik. Modified generalized alpha method for integrating governing equations of very flexible aircraft, AIAA 2006-1747. In *47th AIAA/ ASME/ ASCE/ AHS/ ASC Structures, Structural Dynamics, and Materials Conference, 01-04 May*. AIAA, 2006. doi: 10.2514/6.2006-1747. URL https://arc.aiaa.org/doi/pdf/10.2514/6.2006-1747.

[106] Walter Silva and Robert M. Bennett. Using transonic small disturbance theory for predicting the aeroelastic stability of a flexible wind-tunnel model, AIAA 90-1033-cp. In *31st Structures, Structural Dynamics and Materials Conference, 02-04 Apr.* AIAA, 1990. doi: 10.2514/6.1990-1033. URL https://arc.aiaa.org/doi/pdf/10.2514/6.1990-1033.

[107] Ashok K. Singh and C. W. Nichols. Derivation of an equivalent beam model from a structural finite element model. In *Proceedings of the MSC 1988 World Users Conference*, 1988.

[108] Jennifer J Sitz. Aeroelastic analysis of a joined-wing sensorcraft. Master's thesis, Air Force Institute of Technology, Air University, USAF, 2004. URL http://www.dtic.mil/dtic/tr/fulltext/u2/a426635.pdf.

[109] Christian Spada. Aeroelastic analysis of nonlinear high aspect ratio wings. Master's thesis, Instituto Superior Técnico, 2014.

[110] Weihua Su. *Coupled nonlinear aeroelasticity and flight dynamics of fully flexible aircraft*. PhD thesis, University of Michigan, 2008.

[111] Weihua Su and Carlos E. S. Cesnik. Dynamic response of highly flexible flying wings, AIAA 2006-1636. In *47th AIAA/ ASME/ ASCE/ AHS/ ASC Structures, Structural Dynamics, and Materials Conference, 01-04 May*. AIAA, 2006. doi: 10.2514/6.2006-1636. URL https://arc.aiaa.org/doi/pdf/10.2514/6.2006-1636.

[112] Weihua Su and Carlos E. S. Cesnik. Nonlinear aeroelasticity of a very flexible blended-wing-body aircraft. *Journal of Aircraft*, 47(5):1539–1553, 2010. ISSN 0021-8669 1533-3868. doi: 10.2514/1.47317. URL https://arc.aiaa.org/doi/pdf/10.2514/1.47317.

[113] Weihua Su and Carlos E. S. Cesnik. Strain-based geometrically nonlinear beam formulation for modeling very flexible aircraft. *International Journal of Solids and Structures*, 48(16):2349–2360, 2011. ISSN 0020-7683. doi: 10.1016/j.ijsolstr.2011.04.012. URL http://www.sciencedirect.com/science/article/pii/S0020768311001491.

[114] Weihua Su and Carlos E. S. Cesnik. Strain-based analysis for geometrically nonlinear beams: A modal approach. *Journal of Aircraft*, 51(3):890–903, 2014. ISSN 0021-8669. doi: 10.2514/1.C032477. URL https://doi.org/10.2514/1.C032477.

[115] Erwin Sulaeman, Rakesh Kapania, and Raphael Haftka. Effect of compressive force on strut-braced wing response, AIAA 2001-1611. In *42nd AIAA/ ASME/ ASCE/ AHS/ ASC Structures, Structural Dynamics, and Materials Conference and Exhibit, 16-19 Apr.* American Institute of Aeronautics & Astronautics, 2001. doi: 10.2514/6.2001-1611. URL https://arc.aiaa.org/doi/pdf/10.2514/6.2001-1611.

[116] Deman Tang and Earl H. Dowell. Experimental and theoretical study on aeroelastic response of high-aspect-ratio wings. *AIAA Journal*, 39(8):1430–1441, 2001. ISSN 0001-1452 1533-385X. doi: 10.2514/2.1484. URL https://arc.aiaa.org/doi/pdf/10.2514/2.1484.

[117] Nick Teunisse, Paolo Tiso, Luciano Demasi, and Rauno Cavallaro. Reduced order methods and algorithms for structurally nonlinear joined wings, AIAA 2015-0699. In *56th AIAA/ASCE/AHS/ASC Structures, Structural Dynamics, and Materials Conference, 05-09 Jan.*, 2015. doi: 10.2514/6.2015-0699. URL https://arc.aiaa.org/doi/pdf/10.2514/6.2015-0699.

[118] Ilhan Tuzcu and Leonard Meirovitch. Effects of flexibility on the stability of flying aircraft. *Journal of Dynamic Systems, Measurement, and Control*, 127(1):41–49, 2005. doi: 10.1115/1.1870040.

[119] Marthinus C. Van Schoor and Andreas H. Von Flotow. Aeroelastic characteristics of a highly flexible aircraft. *Journal of Aircraft*, 27(10):901–908, 1990. ISSN 0021-8669 1533-3868. doi: 10.2514/3.45955. URL https://doi.org/10.2514/3.45955.

[120] Marthinus C. Van Schoor, S. H. Zerweckh, and Andreas H. Von Flotow. Aeroelastic stability and control of a highly flexible aircraft, AIAA-89-1187-CP. In *30th Structures, Structural Dynamics and Materials Conference, 03-05 Apr.* AIAA, 1989. doi: 10.2514/6.1989-1187. URL https://doi.org/10.2514/6.1989-1187.

[121] Zhicun Wang, P. C. Chen, D. D. Liu, D. T. Mook, and Mayuresh J. Patil. Time domain nonlinear aeroelastic analysis for HALE wings, AIAA 2006-1640. In *47th AIAA/ ASME/ ASCE/ AHS/ ASC Structures, Structural Dynamics, and Materials Conference, 01-04 May*. AIAA, 2006. doi: 10.2514/6.2006-1640. URL https://arc.aiaa.org/doi/pdf/10.2514/6.2006-1640.

[122] Noud P. M. Werter and Roeland De Breuker. Aeroelastic tailoring and structural optimisation using an advanced dynamic aeroelastic framework. In *IFASD 2015: 16th International Forum on Aeroelasticity and Structural Dynamics, 28 June-2 July 2015*, 2015. URL http://resolver.tudelft.nl/uuid:70031de8-ecc0-4320-a4ce-76a0961b104c.

[123] Noud P. M. Werter, Jurij Sodja, and Roeland De Breuker. Design and testing of aeroelastically tailored wings under maneuver loading. *AIAA Journal*, 55(3):1012–1025, 2016. ISSN 0001-1452. doi: 10.2514/1.J054965. URL https://doi.org/10.2514/1.J054965.

[124] Wei Zhao, Rakesh K. Kapania, Joseph A. Schetz, and John M. Coggin. Nonlinear aeroelastic analysis of SUGAR truss-braced wing (TBW) wind-tunnel model (WTM) under in-plane loads, AIAA 2005-1173. In *56th AIAA/ASCE/AHS/ASC Structures, Structural Dynamics, and Materials Conference, 05-09 Jan.* AIAA, 2015. doi: 10.2514/6.2015-1173. URL https://arc.aiaa.org/doi/pdf/10.2514/6.2015-1173.

[125] Zhenjun Zhao and Gexue Ren. Multibody dynamic approach of flight dynamics and nonlinear aeroelasticity of flexible aircraft. *AIAA Journal*, 49(1):41–54, 2011. ISSN 0001-1452 1533-385X. doi: 10.2514/1.45334. URL https://arc.aiaa.org/doi/pdf/10.2514/1.45334.